Reviewing chronostratigraphic uncertainty of the Ediacaran-Cambrian transition

Fred T. Bowyer[1,†,*], Lyle Nelson[2, †,*]

[1]*School of Earth and Environment, University of Leeds, Leeds, LS2 9JT, UK*

[2]*Department of Earth, Atmospheric and Planetary Sciences, Massachusetts Institute of Technology, Cambridge, MA 02139, USA*

[†]These authors contributed equally

*Correspondence: Fred Bowyer (f.t.bowyer@leeds.ac.uk), Lyle Nelson (llnelson@mit.edu)

ABSTRACT

The Ediacaran-Cambrian transition archives the widespread disappearance of 'Ediacaran-type' soft-bodied biota and the appearance of most modern animal body plans, including a major diversification of skeletal animals and styles of animal-substrate interaction. Despite over a century of study, our ability to confidently reconstruct the series of macroevolutionary events that inform origination and extinction rates across the Ediacaran-Cambrian transition is challenged by underlying ambiguity in global stratigraphic correlation. Here, we review the chronology of events recorded by the successions that are currently the most temporally well-constrained, discuss major uncertainties, and use this perspective to reconstruct plausible global age frameworks for published biostratigraphic and chemostratigraphic data. Current models support minor temporal overlap of classically Ediacaran and Cambrian calcified animal fossils, aid assessments of eustatic sea-level and drivers of carbon isotope instability, contextualize regional datasets, and highlight the approaches required for further refinement. While there remains ~5 million years of uncertainty, holistic evaluation of existing chronostratigraphy suggests that the GSSP for the Ediacaran-Cambrian boundary falls between 538 and 533 Ma.

Keywords: Ediacaran, Cambrian, Geochronology, animal evolution, GSSP

Linking Ediacaran-Cambrian life and environment

Sedimentary rocks of Ediacaran age [ca. 635 million years ago (Ma) to between 538 Ma and 533 Ma] host the first record of complex and morphologically differentiated macrofossils, including the earliest animals (Fig. 1a, e.g., Gold et al., 2015; Dunn et al., 2021). Strata from the final ca. 12–18 Myrs of the Ediacaran also contain the first evidence for animal biomineralization (Germs, 1972), which was then widely adopted during the canonical 'Cambrian Explosion' (Matthews and Missarzhevsky, 1975) – a major increase in animal diversity and morphological complexity in the lower Cambrian that included the appearance of

most extant animal body plans (Fig. 1a, b). Our understanding of how Ediacaran and Cambrian communities are related is incomplete, however, because the affinities of most Ediacaran fossil biota remain uncertain. The degree and tempo of biotic turnover across the Ediacaran-Cambrian transition also remains veiled by spatial, temporal, and taphonomic uncertainties and biases of the preserved fossil record.

The synchronous co-option of key innovations (e.g., body plan differentiation, biomineralization) by independent lineages is hypothesized to reflect the operation of external, environmental triggers (e.g., Erwin, 2021). While many have been proposed, the pre-eminent environmental trigger for Ediacaran-Cambrian innovation is often linked with a possible increase in oxygen and/or nutrient availability required to fuel energetically costly metabolisms including motility, predation, and biomineralization (e.g., Stockey et al., 2024 and references therein). Changing seawater chemistry has also been proposed as an environmental trigger for early animal biomineralization, which may have been under minimal biological control (e.g., Wood et al., 2017). Thereafter, rapid diversification of lower Cambrian fossil assemblages was linked to a cascade of ecological interactions, including an increase in the complexity of predator-prey dynamics and ecological engineering (e.g., Bengtson, 2002; Sperling et al., 2013; Darroch et al., 2021). While each of these factors likely played a role, the degree to which we are able to accurately reconstruct the stratigraphic record in space and time places limitations on our ability to test hypotheses that link biotic and environmental change.

Global chronostratigraphic frameworks have the potential to yield a coherent and globally representative temporal narrative to integrate data streams (e.g., temporally calibrated chemostratigraphic and biostratigraphic records, Fig. 1d; Maloof et al., 2010; Bowyer et al., 2022; Nelson et al., 2023). The achievable resolution of this record is tempered by the completeness of the rock record, and particularly by the availability of carbonate rocks, fossil-preservation windows, and material suitable for absolute age determination via radioisotope

geochronology. Here, we review recent progress and ongoing challenges associated with global stratigraphic correlation across the Ediacaran-Cambrian transition. By focusing on sections with high-precision age constraints, we present the current chronostratigraphic scaffold for the extrapolation of global age frameworks that temporally calibrate and visualize recent community-wide research efforts. Aspects common to both frameworks allow us to address some unresolved issues, while also illuminating the largest remaining uncertainties that require targeted future study to resolve.

Defining characteristics of the Ediacaran-Cambrian transition

The base of the Cambrian is defined by the lowest stratigraphic occurrence (LO) of the trace fossil *Treptichnus pedum* in the ratified Global boundary Stratotype Section and Point (GSSP) at Fortune Head, on the Burin Peninsula of Newfoundland, Canada (Brasier et al., 1994). It is widely acknowledged that the lowest occurrence of a fossil rarely, if ever, corresponds to the first appearance of the respective organism due to palaeoenvironmental, preservational and collection biases (e.g., Gehling et al., 2001). Consequently, many researchers now consider the base of the *T. pedum* ichnofossil assemblage Zone (IAZ, a collection of co-occurring trace fossils that includes *T. pedum*), to more accurately mark the base of the Cambrian (e.g., Landing et al., 2013; Geyer and Landing, 2017). At the GSSP level, the base of the *T. pedum* IAZ marks a notable increase in the diversity of trace making ecologies (Gougeon et al., 2025a, b).

The succession at Fortune Head is readily accessible, characterized by continuous deposition without recognized hiatuses, and records a progressive sequence of ichnofossil assemblages whose lowest occurrences show limited evidence for facies control (Geyer and Landing, 2017; Gougeon et al., 2025b); all features that are highly desirable for GSSP assignment (Brasier et al., 1994). And yet, several aspects of the GSSP have complicated direct extrapolation of important boundary characteristics to other globally distributed successions

(e.g., Babcock et al., 2014). Most notably, the Burin Peninsula is dominated by siliciclastic sedimentary rocks where laterally continuous carbonate interlayers do not occur until several hundred meters above the GSSP level (Myrow and Hiscott, 1991). The paucity of carbonates hinders comparison of the GSSP with carbonate-dominated successions elsewhere, as there is limited potential for (1) biostratigraphic correlation of shelly fossils, and (2) direct correlation of boundary-defining features via carbonate chemostratigraphy [e.g., through use of carbonate carbon isotopes ($\delta^{13}C_{carb}$)]. Meanwhile, carbonate-dominated successions in other regions may lack siliciclastic interlayers that preserve the defining trace fossils of the boundary interval, but host carbonates with chemostratigraphic potential and distinct fossil biotas [e.g., small skeletal/shelly fossils (SSFs)] that are a hallmark of early Cambrian animal radiation. These issues have led several researchers to advocate for the use of auxiliary markers to help identify Ediacaran vs Cambrian strata, including the LO of Cambrian-type SSFs, the disappearance of Ediacaran-type soft-bodied and/or calcified macrofossils, and a chemostratigraphic marker termed the 'BAsal Cambrian carbon isotope Excursion' (BACE, e.g., Zhu et al., 2006; Landing et al., 2013; Geyer and Landing, 2017).

Aside from the defining characteristics of the boundary itself, two additional aspects complicate accurate global spatiotemporal calibration across the Ediacaran-Cambrian transition. First, this interval is widely recognised to coincide with major sequence boundaries in the majority of globally distributed successions, with sedimentary rocks that host Cambrian-type SSFs and ichnofossils often being separated from underlying strata by erosional surfaces that represent unconformities of unknown duration. Indeed, on many cratons, the onset of Cambrian deposition is transgressive and diachronous (e.g., Runnegar et al., 1995; Shahkarami et al., 2020), which is exemplified in Laurentia near the base of the Sauk transgression (Sloss, 1963; Karlstrom et al., 2020; Nelson et al., 2023).

Second, while a series of maximum depositional ages for correlative strata in New Brunswick suggest a boundary age of >531.53 ± 0.28 Ma (e.g., Isachsen et al., 1994; Barr et al., 2022; Hamilton et al., 2023), the GSSP itself lacks high-resolution radioisotopic age constraints. Lower Cambrian sedimentary successions, more broadly, suffer from a general paucity of ash beds for zircon U-Pb age dating (Box 1, Fig. 2, Table S1). This means that the absolute age for the Ediacaran-Cambrian boundary on international chronostratigraphic charts is poorly constrained, debated, and ripe for revision through incremental advancements in regional stratigraphic frameworks and inter-regional correlations between sections that host datable rocks and fossil occurrences (e.g., Linnemann et al., 2019; Hodgin et al., 2021; Nelson et al., 2022, 2023, in press; Bowyer et al., 2025).

As should be expected, no single section comprising mixed carbonate-siliciclastic strata hosts all the features required to robustly anchor the full sequence of evolutionary events across the Ediacaran-Cambrian transition in absolute time. To complicate things further, ambiguity in lithostratigraphic and $\delta^{13}C_{carb}$ correlation can also yield notably different estimates for the degree of temporal overlap between Ediacaran and Cambrian fossil assemblages, thereby hampering a robust evaluation of origination and extinction rate across the boundary (e.g., Zhu et al., 2017; Nelson et al., 2023; Bowyer et al., 2023a). Reducing these uncertainties therefore requires careful integration of multiple datasets from globally distributed boundary strata (e.g., Lindsay et al., 1996; Landing et al., 2013; Babcock et al., 2014; Geyer and Landing, 2017). Below, we outline and visualize one such framework to help resolve evolutionary and geochemical changes across this interval of biosphere revolution.

Text for Box 1:

Interpreting near-depositional versus maximum depositional ages from zircon U-Pb geochronology

Single grain zircon U-Pb chemical abrasion-isotope dilution-thermal ionization mass spectrometry (CA-ID-TIMS, Mattinson, 2005) affords the highest level of precision and accuracy of all radioisotopic methods for deep time calibration (Condon et al., 2024; Yang et al., 2025). However, multiple factors have to be considered before interpreting the geologic significance (e.g., depositional age) of radioisotopic date(s) from a given sample. These include the degree of physical reworking of zircon grains in the dated horizon (through sedimentary or volcanic processes), compositional variability within the dated horizon that reflects heterogenous ages of zircon grains within a magma chamber and/or source area, potential biases introduced through physical separation and optical selection of zircon grains, and the full range of precision afforded by the analytical methodology, tracer calibration and U decay constant uncertainties (Condon et al., 2024).

CA-ID-TIMS laboratories around the world have significantly reduced inter-laboratory methodological uncertainties by sharing EARTHTIME multi-isotope tracer solutions (Condon et al., 2015), which have (1) resulted in unprecedented precision and accuracy on individual weighted mean zircon U-Pb dates, with analytical uncertainties that are commonly as low as ±0.05% (Schaltegger et al., 2015), and (2) effectively eliminated inter-laboratory analytical variability for zircon U-Pb CA-ID-TIMS measurements (Symanowski et al., 2025). However, the aforementioned issues of zircon grain selection, physical reworking and complex zircon grain populations within dated horizons mean that reported ages cannot always be assumed to approximate near-depositional ages (e.g., Bowyer et al., 2025). While weighted mean ages from volcanic zircon grains in ash beds are commonly interpreted to approximate near-depositional ages, this is heavily dependent upon whether the dated grains represent the youngest (autocrystic) population in the magma chamber as opposed to a dominant proportion of older (antecrystic) grains or exogenic (xenocrystic) grains present in the magma chamber prior to eruption (e.g., Keller et al., 2018), or incorporated as epiclastic components during

transport and deposition (Ramezani et al., 2011). Alternatively, maximum depositional ages are interpreted based on youngest zircon grain populations in either sedimentary beds or tuffs with epiclastic components (e.g., Hodgin et al., 2021; Nelson et al., 2023) or from superposition relationships above dated igneous or volcanic bodies. Robustly interpreting the geologic significance of a high-precision age therefore requires careful consideration of a multitude of factors from outcrop to grain-scale as well as laboratory methodology and data spread, with the latter often benefiting from statistical approaches to characterize and identify zircon population distributions.

View of the boundary interval from radioisotopically calibrated sections

Here, we collate a series of published high-precision zircon U-Pb ages from uppermost Ediacaran through lower Cambrian strata on multiple continents and interpret their reliability to inform near-depositional versus maximum depositional ages for associated data in each section (Figs. 2 and 3, Table S1). We also preliminarily extrapolate this record through comparison of data from two sections that lack absolute age constraints but contain 1) the GSSP for the Cambrian base (Fortune Head, Avalonia), and 2) chemostratigraphically calibrated regional lowest occurrences of Cambrian-type SSFs (Bayan Gol, Zavkhan Terrane, Mongolia), which are presently lacking from all sections that are calibrated by radioisotope geochronology (Fig. 3). While this approach does not initially consider data from other sections/successions that host important fossil occurrences and chemostratigraphic records (e.g., South China, Siberian Platform, Iberian Zone, Morocco), it allows us to construct a reliable age-calibrated base (skeleton) framework from multiple globally distributed areas that informs a catalogue of calibrated fossil last and first appearances along with trends in chemostratigraphic data. This base framework can then be used as a tool for global correlation (Figs. 3 and 4).

The age of the BACE

Data from the Ara Group of Oman have previously been used to prescribe an age of ca. 541 Ma for the onset of the BACE and the disappearance of the Ediacaran biomineralized animals *Cloudina* and *Namacalathus* (Fig. 3, e.g., Amthor et al., 2003; Bowring et al., 2007). Lithostratigraphic correlations between Ara Group drill cores are complicated by the structure of carbonate deposits within the basin, which are preserved as stringers bounded by evaporite strata. The nature of mixed carbonate-evaporite deposition suggest that some intervals may record temporary restriction that could enhance local isotope reservoir effects (e.g., Lazar and Erez, 1990) or bias the fossil record. The fidelity of associated $\delta^{13}C_{carb}$ data to record trends in open marine composition is therefore uncertain. Furthermore, there may be stratigraphic hiatuses, as intervals of exposure/dissolution are common in evaporitic environments (e.g., Schröder et al., 2005), which adds a challenge to age model construction. The resolution of published geochemical and palaeontological data also varies significantly between core profiles, complicating regional correlations. As a result, a zircon U-Pb CA-ID-TIMS age derived from a tuff interbed in one core cannot always be used with confidence to temporally calibrate data from a neighbouring core. Despite these complications, the A3 carbonate member of the Ara Group hosts positive $\delta^{13}C_{carb}$ values that are temporally calibrated between 542.90 ± 0.12 and 542.33 ± 0.12 Ma (Bowring et al., 2007) and are similar to positive values reported from open marine carbonates of the upper Tamengo Formation, Brazil that are ca. >541.85 ± 0.75 Ma and of the upper Nudaus and basal Urusis formations of the Nama Group, Namibia that are >542.65 ± 0.15 Ma (Fig. 3, Saylor et al., 1998; Boggiani et al., 2003; Parry et al., 2017; Ramos et al., 2022; Nelson et al., 2022).

A tuff bed at the base of the A4 (“U”) carbonate member of the Ara Group yields a high-precision CA-ID-TIMS age of 541.00 ± 0.13 Ma (Fig. 3, Bowring et al., 2007). This was previously used as a minimum age constraint for the disappearance of *Cloudina* and *Namacalathus*, and the age of BACE onset (Amthor et al., 2003; Bowring et al., 2007).

However, cloudinids/cloudinomorphs have since been reported from non-evaporitic marine carbonates as young as 538.56 +0.08/−0.09 Ma on the Kalahari craton, where evidence for the BACE is lacking (Fig. 3, Nelson et al., 2022). The zircon U-Pb CA-ID-TIMS date of the ash bed at the base of the A4 Member may represent a near-depositional age. However, this should only be considered a maximum depositional age for onset of the BACE due to its relative position beneath carbonates that record the excursion, the possibility for depositional hiatus and/or condensed deposition between the ash layer and overlying carbonate (see detailed appraisal in Nelson et al., 2023), and the possibility for local isotope reservoir effects in the South Oman Salt Basin. The weight of evidence from open marine mixed carbonate-siliciclastic strata of the Kalahari Craton currently suggests an onset age for the BACE <537.9 Ma (Fig. 3, Nelson et al., 2022, in press). This interpretation is also consistent with a maximum depositional age of ≤539.40 ± 0.23 Ma from the stratigraphic interval recording the nadir of the BACE within sections exposed in Sonora, Mexico (Fig. 3, Hodgin et al., 2021). Carbon isotope and biostratigraphic data from southwestern Laurentia also constrain the regional last appearance of cloudinomorphs and soft-bodied erniettomorphs stratigraphically below the BACE nadir (Hodgin et al., 2021; Smith et al., 2016a, 2023; Nelson et al., 2023).

***First appearance of* T. pedum**

In all mixed carbonate-siliciclastic successions that host both the BACE and *T. pedum*, the stratigraphically lowest known *T. pedum* occur above the BACE nadir, and closely above the level of a muted $\delta^{13}C_{carb}$ peak, recently termed '1.5p' (Narbonne et al., 1994; Knoll et al., 1995; Corsetti and Hagadorn, 2003; Landing et al., 2013; Smith et al., 2016a, 2016b, 2017; Geyer and Landing, 2017; Etemad-Saeed et al., 2021; Hodgin et al., 2021; Bowyer et al., 2022, 2023b, 2024; Nelson et al., 2022, 2023; Topper et al., 2022; Zhang et al., 2024; Marusin, 2025). Two sections of the Great Basin, Laurentia, contain shallow marine clastic beds that incorporated relatively young zircon grains through either typical sediment transport or as ash fall, which

have been dated to provide maximum depositional ages through a combination of zircon screening via laser ablation inductively coupled mass spectrometry analyses and subsequent CA-ID-TIMS of youngest grain populations (Hodgin et al., 2021; Nelson et al., 2023). It is important to stress that none of these ages can be confidently interpreted to represent depositional ages (contra Runnegar et al., 2025, see box 1). Instead, these together constrain a maximum depositional age of ≤539.40 ± 0.23 Ma for the BACE nadir and ≤532.83 ± 0.98 Ma for the regional lowest occurrences of *T. pedum*, *Psammichnites*/*Taphrhelminthopsis*, and arthropod trace fossils (Fig. 3, Hodgin et al., 2021; Nelson et al., 2023; Jensen et al., 2002). The latter maximum depositional age presently remains the best approximation for the age of the Ediacaran-Cambrian boundary, based on the defining characteristics of the GSSP (Fig. 3). As reviewed previously, ages of strata in New Brunswick imply that the regional lowest occurrence of *T. pedum* in Avalonia is >531.53 ± 0.28 Ma (Hamilton et al., 2023), which is consistent with the first appearance of this index ichnotaxon at ~533–532 Ma.

First appearance of Cambrian-type SSFs

A challenge to correlation of the existing Great Basin record is the paucity/absence of earliest Cambrian, pre-Series 2 SSFs, which are recorded from carbonates in other regions in proximity to the BACE (e.g., Siberia, South China, Mongolia; Brasier et al., 1996; Steiner et al., 2007; Maloof et al., 2010; Smith et al., 2016b; Li et al., 2013; Bowyer et al., 2022, 2023a and references therein; Topper et al., 2022). Nevertheless, extrapolating trends in $\delta^{13}C_{carb}$ data from the Great Basin to carbonate-dominated successions that host diverse SSF records suggests that, in some regions, SSFs may indeed have appeared in advance of, or broadly coincident with, the first appearance of *T. pedum* (Fig. 3). Perhaps the most conservative estimate for the minimum age of SSF first appearances is derived by extrapolation to the Bayan Gol section of the Zavkhan Terrane, Mongolia (Smith et al., 2016b; Topper et al., 2022; Fig. 3). There, $\delta^{13}C_{carb}$ data exhibit an initial decrease prior to the BACE that correlates well with

the most complete sections of the Great Basin (e.g., Mount Dunfee, Smith et al., 2016a) and the record from the Central Iberian Zone, Spain (Zhang et al., 2024). This initial negative $\delta^{13}C_{carb}$ trend below the nadir of the BACE, which was previously referred to as '0n' (Bowyer et al., 2023a), has recently been termed the 'late Ediacaran Negative carbon Isotope Plateau' (ENIP, Zhang et al., 2024), which we adopt here. Importantly, the ENIP is only recorded in sections/successions where sedimentation rates appear to have been high and is absent or extremely condensed in areas (e.g., most sections of South China) where sedimentation rates were low. Strata below the onset of negative values within the 'late Ediacaran Positive carbon Isotope Plateau' (EPIP), as well as within the ENIP below the nadir of the BACE, host occurrences of a number of novel cloudinomorph morphologies in the Great Basin (e.g., *Saarina*, *Costatubus*, Selly et al., 2020; Schiffbauer et al., 2024) and Zavkhan Terrane (*Zuunia*, Yang et al., 2020; Topper et al., 2022), of which the latter certainly extends into the lower Cambrian, post-BACE (Topper et al., 2022). Given that these occurrences represent exceptional preservation via pyritization, and are facies controlled (e.g., Selly et al., 2020; Smith et al., 2023), it remains unclear how globally widespread or long-ranging these novel morphologies actually were within the terminal Ediacaran. The ENIP interval of the Zavkhan Terrane may also host the lowest occurrence of SSFs in the form of the morphologically simplest anabaritid *Cambrotubulus* (which may also occur within this interval in some sections of Siberia, see below), but the affinity of this specimen remains uncertain (Fig. 3, Topper et al., 2022). Last, the lowest occurrence of protoconodonts (another group of Cambrian-type SSFs) in the Zavkhan Terrane coincides with rising $\delta^{13}C_{carb}$ values above the BACE nadir (Topper et al., 2022), shortly pre-dating or approximately coinciding with the lowest occurrence of *T. pedum* based on visual alignment of $\delta^{13}C_{carb}$ data with the Great Basin record.

On the Siberian Platform, regional lowest occurrences of Fortunian SSFs are recognized to be under partial lithological control associated with poor preservation during early

dolomitization versus phosphatization/glauconitization within limey dolostone/limestone interbeds (e.g., Kouchinsky et al., 2017; Bowyer et al., 2023a; Marusin et al., 2023). By contrast, preservational conditions that promoted phosphogenesis/glauconitization, such as upwelling and/or stratigraphic condensation, appear to have been absent from the southwestern Laurentian margin in the basal Cambrian. Previous studies have inferred palaeobiogeographic trends from spatial distributions of SSF first occurrences, including inferences of first occurrence in Siberian or Mongolian terranes prior to global dispersal (e.g., archaeocyath distribution, Zhuravlev, 1986; Maloof et al., 2010). However, a recent report of exceptionally preserved archaeocyath specimens in the basal Kuanchuanpu Formation at Zhangjiagou, South China, which appear to derive from Fortunian strata, may instead suggest that some geographic differences could simply reflect preservational biases on phosphatization/glauconitization (Wang et al., 2025). The precise age of the Kuanchuanpu lagerstätte in the Zhangjiagou section is dependent upon regional biostratigraphic correlation only and additional lines of evidence are required to robustly demonstrate a basal Fortunian age for these fossils (e.g., Wang et al., 2025 and references therein).

Auxiliary ichnofossil markers for the Cambrian base

At the Cambrian GSSP, the base of the *T. pedum* IAZ is above the regional lowest occurrence of *T. pedum* and above the last occurrence of the problematic body fossil *Harlaniella podolica* within lower Member 2 of the Chapel Island Formation (Fig. 3, Landing et al., 2013; Geyer and Landing, 2017; Gougeon et al., 2025b). Aside from *T. pedum*, other ichnotaxa that occur above the base of Member 2 at Fortune Head, immediately below or significantly above the *H. podolica – T. pedum* IAZ boundary, but are not known from the dated mixed carbonate-siliciclastic succession on the Neint Nababeep Plateau (or from other contemporaneous deposits of the Kalahari craton) include *Gyrolithes*, *Teichichnus* and arthropod traces (Darroch et al., 2021; Nelson et al., 2022, in press; Gougeon et al., 2025b).

These represent examples of new architectural designs that document the appearance of novel lower Cambrian body plans (e.g., Mángano and Buatois, 2020) and have the potential to serve as auxiliary ichnotaxa for the identification of Fortunian strata. Meanwhile, *Monomorphichnus*, *Psammichnites*, and *Cochlichnus* -like traces, as well as *Gordia*, may predate the BACE nadir and regional lowest occurrences of *T. pedum* (e.g., Buatois and Mángano, 2016; Darroch et al., 2021; Nelson et al., 2022; Turk et al., 2022; Azizi et al., 2023). Indeed, other obviously bilaterian trace fossils showing significant ranges of complexity and size significantly predate the calibrated range of the *T. pedum* IAZ and the BACE with well calibrated occurrences of ichnotaxa such as treptichnids, *Archaeonassa*, *Parapsammichnites*, and *Streptichnus* on the Kalahari craton between c. 541 and 538 Ma (e.g., Linnemann et al., 2019; Darroch et al., 2021; Nelson et al., 2022, in press; Bowyer et al., 2025; Gong et al., 2025). Linnemann et al. (2019) argued some of these trace fossils could be taken to mark the base of the Cambrian, and as such applied an age of 538.8 Ma to the GSSP, which has subsequently appeared in numerous publications and chronostratigraphic charts. We emphasize that, given the documented multi-million-year overlap of some of these ichnotaxa and Ediacaran body fossils of the Nama assemblage and lack of ichnotaxa of the *T. pedum* IAZ, this level/age is not obviously correlative to the current GSSP (see detailed discussion in Nelson et al., in press). Furthermore, if the community decides a broader assemblage of bilaterian trace fossils should instead mark the base of the Cambrian, the lowest occurrences of such fossils are nearly 1 km lower in the Nama Group at ~541 Ma (e.g., Turk et al., 2022; Gong et al., 2025) and >500 meters below the BACE and lowest occurrence of *T. pedum* in Nevada (Tarhan et al., 2020).

Global chronostratigraphic frameworks

Datable ash beds are not evenly distributed in space and time, and (for this interval of the geologic record) an approach that uses youngest detrital zircon populations to provide

maximum depositional age estimates is in its infancy. The dated sections displayed in figure 3 offer an exceptional multi-proxy record to constrain the co-evolution of life and environment across the Ediacaran-Cambrian transition but they offer only a partial snapshot of full global ecospace. The palaeontological record of any section is controlled by a number of local effects, including changes in regional palaeoenvironmental conditions (e.g., oxygen or nutrient availability), changes in the distribution of preserved environmental settings (e.g., nearshore siliciclastic versus carbonate platform) and changes in the suitability of post-depositional microenvironments for fossil preservation (e.g. taphonomic windows that promote authigenic phosphate, pyrite, or clay minerals). Likewise, the fidelity of the geochemical record to archive changes in global ocean composition is determined by the degree of regional restriction as well as diagenetic effects (e.g., Ahm and Husson, 2022, and references therein). A holistic appreciation of global change across the Ediacaran-Cambrian transition necessitates that the skeleton age framework built using well-dated sections is extrapolated to incorporate data from as many globally distributed sections as possible. However, each of these regional syn- and post-depositional effects must be considered during the process of extrapolation, on a case-by-case basis. By correlating long-term trends in $\delta^{13}C_{carb}$ (rather than absolute magnitudes), the resulting global age framework visualizes the full compositional range in $\delta^{13}C_{carb}$ across individual excursions. It also pins all palaeontological information from carbonate or mixed carbonate-siliciclastic succession to the radioisotopically calibrated compilation. Palaeontological data are also incorporated from siliciclastic-only successions with radioisotopic dated interbeds, while additional biotic datasets from successions that are poorly constrained in time are assigned preliminary age ranges based on biostratigraphic best fit to the temporally calibrated prior framework.

Chemostratigraphic correlation

Figure 4 shows two possible global age frameworks that cover the Ediacaran-Cambrian transition from 556 Ma to 528 Ma (full data and references in Table S2). Both were constructed using a hierarchical methodology that first considers all regional lithostratigraphic, chemostratigraphic and palaeontological information to develop regional composite profiles. The temporal calibration of regional composites was then achieved through correlation (via visual alignment of $\delta^{13}C_{carb}$) to sections that host $\delta^{13}C_{carb}$ data anchored by dated interbeds (e.g., Maloof et al., 2010; Bold et al., 2016; Yang et al., 2021; Bowyer et al., 2022, 2023a,b, 2024, 2025). This established chemostratigraphic approach relies on the basic assumption that marine $\delta^{13}C_{carb}$ trends are relatively globally consistent. Moreover, this exercise is wholly iterative, meaning that many aspects of previous age frameworks (e.g., BACE calibrations of Maloof et al., 2010; Bowyer et al., 2022) are incompatible with more recently reported data and updated correlation interpretations (e.g., Bowyer, 2023, 2024; Nelson et al., 2023, and this study).

The principal difference between the two presented age frameworks is the duration of the BACE, with an onset timing that may be as late as ca. 533 Ma (onset age for short-duration BACE Model 1 is set at 535 Ma on the assumption that sedimentation rates are roughly uniform across the BACE and through overlying strata, Fig. 4a, Nelson et al., 2023; Bowyer et al., 2024) or as early as ca. 538 Ma (long-duration BACE Model 2, Fig. 4b). Differences in the onset timing and duration affect the temporal coincidence of specific external events that have been suggested as drivers for the BACE and influence how these data are applied towards carbon cycle modelling. As the tightest constraints pinning the BACE right now are ≤ ca. 538 Ma for the onset (Nelson et al., 2022, in press) and ≤ ca. 533 Ma for the recovery (Nelson et al., 2023), the timespan of the BACE cannot be further distinguished between these endmembers at present. This precludes robust interpretation of the length of the BACE, which could be interpreted from a ca. 5 Myr to a sub-1 Myr timescale—clearly with different implications for carbon cycle dynamics.

Ediacaran-Cambrian biotic overlap and extinction/origination

Rescaling the BACE duration also impacts temporal interpretations of biostratigraphic data from some sections in the pre-BACE interval, which has downstream effects on both associated biotic range data and origination and extinction rates interpreted using mean generic richness (e.g., using methods outlined in Bowyer et al., 2024). Specifically, in Model 2 the timing of any extinction event would occur earlier than in Model 1, which could imply that extinction occurred over a more protracted interval than Model 1 and/or that terminal Ediacaran extinction and Fortunian origination were significantly separated, temporally (Fig. 4a, 4b). The reason for this is that the timing of any extinction pulse in this interval is controlled by the last occurrences of soft-bodied Ediacaran fauna in advance of the BACE nadir. As previously noted, however, extinction rates interpreted for any such model are exaggerated by very low mean generic richness prior to BACE onset (Bowyer et al., 2024). The extinction of soft-bodied Ediacaran fauna might also coincide with an interpreted interval of terminal Ediacaran origination, which broadly corresponds to the lowest occurrence of novel cloudinomorph genera in sections of the Great Basin and Mongolian Zavkhan Terrane (e.g., Selly et al., 2020; Yang et al., 2020). Importantly, it is inherently difficult to estimate diversity within morphologically simple morphoclades, such as tubular forms, that either lack distinct diagnostic features or commonly have poor preservational quality (e.g. Selly et al., 2020). This underlying uncertainty in how to define taxa and lump/split fossils is compounded with the uncertainties in timescale/range-distribution outlined in this review, on top of the fundamental taphonomic biases. As a result of these challenges, interpreted patterns in origination/extinction rates may not accurately represent evolutionary history.

The underlying global chemostratigraphic correlation that informs occurrence ages in the biotic dataset (Table S2) assumes minimal overlap of Ediacaran and Cambrian assemblages, thereby potentially exaggerating interpreted peaks in extinction and origination. Minimal

399 overlap is supported by a coherent succession of Fortunian SSF appearances through all
400 individual Cambrian sections/successions (e.g., Topper et al., 2022 and references therein).
401 Nevertheless, some issues remain unresolved and require focused attention in future studies.
402 For example, stratigraphic correlations across the Siberian craton suggest that some of the
403 oldest Cambrian-type SSFs occur immediately pre-BACE nadir, possibly within or even
404 immediately in advance of, the ENIP (e.g., Nagovitsin et al., 2015; Marusin et al., 2023;
405 Bowyer et al., 2023a and references therein). As noted above, preservational issues associated
406 with early dolomitization or lack of authigenic phosphatization partially obscure lowest
407 occurrences of Cambrian SSFs across the Siberian craton (and globally), and regional lowest
408 occurrences are likely to underestimate the age of first appearances (Kouchinsky et al., 2017;
409 Bowyer et al., 2023a; Marusin et al., 2023).

410 There also remain uncertainties in stratigraphic correlation of important sections, especially
411 in southeastern Siberia. In particular, the Kyra-Ytyga section hosts anabaritids that co-occur
412 with cloudinomorphs prior to the first appearance of numerous SSF taxa of the Fortunian
413 *Purella antiqua* assemblage Zone, and all of these are reported from carbonates with positive
414 but decreasing $\delta^{13}C_{carb}$ previously interpreted to correlate with the onset of the BACE (Zhu et
415 al., 2017). Extrapolating such a pre-BACE chemostratigraphic correlation would result in a
416 pronounced pre-BACE peak in origination which, as noted by previous authors, would
417 significantly increase the age of first appearance of several SSF taxonomic groups, including
418 hyoliths, halkieriids and chancelloriids (Zhu et al., 2017; Topper et al., 2022). In this
419 correlation, the first appearance of these SSFs on the Siberian Platform would predate their
420 lowest occurrences in Mongolia and South China by up to several million years. An alternative
421 interpretation is that the Kyra-Ytyga record contains one or more cryptic hiatuses in the upper
422 part of the Ust'-Yudoma Formation, or that its positive $\delta^{13}C_{carb}$ values correlate with peak 5p
423 (Fig. 4, Bowyer et al., 2023a).

Despite these uncertainties, the Kyra-Ytyga section does record the co-occurrence of cloudinomorphs and anabaritids at the same level (Zhu et al., 2017). Conservative models (e.g., Fig. 4) therefore necessitate range extension of cloudinomorphs into the Cambrian. Although *Cloudina* are not known to co-occur with *T. pedum* in lower Cambrian mixed siliciclastic-carbonate successions, various cloudinomorph genera have been reported from carbonate-dominated successions interpreted as lower Cambrian in age based on co-occurrence with Cambrian-type SSFs and/or their stratigraphic occurrences relative to regional $\delta^{13}C_{carb}$ records (e.g., Yang, B. et al., 2016, 2020, 2021; Cai et al., 2019; Topper et al., 2022; Luo et al., 2024). The late Ediacaran diversification of cloudinomorphs and other tubular fauna therefore included survivor/'holdover' taxa, which persisted through terminal-Ediacaran extinction and effectively bridged Ediacaran and Cambrian biotic records. We echo Schiffbauer et al. (2022) and Darroch et al. (2023) who note that continued systematic research into the affinities of the terminal Ediacaran and lower Cambrian skeletal fauna is needed to better understand these patterns of diversity origination and extinction.

Relative versus eustatic sea level change through the transition

Figure 3 shows interpreted base level curves for stratigraphic sections of the Kalahari craton (after Nelson et al., 2022), the Avalonian microcontinent (after Myrow and Hiscott, 1993), the Great Basin (after Smith et al., 2023), and the Zavkhan basin (after Smith et al., 2016b). Interpreting eustatic sea level change from regional depositional records is complicated by the fact that successions in each area document varying subsidence rates that are influence by different regional tectonic processes (e.g., active foreland basin setting for sections of the Kalahari craton, Mongolia, and Oman, and rift basin setting for sections of western Laurentia). However, a general shallowing-upward trend has long been recognized through numerous successions in advance of the BACE (e.g., Runnegar et al., 1995), especially in settings where subsidence rates are likely to have been lower.

In the presented age models, a pulse of regional foreland subsidence led to rapid sediment deposition in the upper Schwarzrand Subgroup of the Nama Group on the western Kalahari craton in the lead up to the BACE (Fig. 3, Nelson et al., 2022, in press). However, elsewhere, eustatic sea level fall during this interval is perhaps supported by erosion of carbonates that record a decreasing trend in $\delta^{13}C_{carb}$, which is interpreted to represent the onset of the ENIP (e.g., upper Turkut Formation of the Siberian craton, Dengying Formation of the Yangtze Platform, South China, and Risky Formation of northwestern Canada). Indeed, the limited preservation of the BACE to marginal tectonically active basins such as the Zavkhan basin of Mongolia or southwestern Laurentia (rather than across widespread epeiric seas) is consistent with a hypothesis that this excursion coincided with a relative eustatic low stand. Pulsed sea level rise is locally recorded during the uppermost ENIP and across the BACE, which is evident from diachronous transgressive flooding seen on the Siberian craton (Bowyer et al., 2023a), in southwestern North America (Smith et al., 2023), in Morocco (Maloof e al., 2005), and in Mongolia (Smith et al., 2016b). While eustasy may have played a role, in each of these cases it is challenging to distinguish this from local tectonic subsidence. Subsequent widespread eustatic sea level rise that postdated the BACE is most apparent from the base of the Sauk Megasequence in Laurentia, in which siliciclastics were deposited atop crystalline basement during diachronous transgression across North America ≥3 Myrs after the BACE (Fig. 4, Sloss, 1963; Keller et al., 2012; Nelson et al., 2023; Tasistro-Hart and Macdonald, 2023). The onset of the Sauk transgression is also apparent in the GSSP succession, within strata of the *T. pedum* IAZ (Fig. 3).

Possible drivers for Ediacaran-Cambrian palaeoenvironmental change

What caused the BACE?

Numerous mechanisms have been put forward to explain large amplitude carbon isotope variability of the late Ediacaran through early Cambrian (e.g., Brasier and Lindsay, 2001; Maloof et al., 2010; Schrag et al., 2013; Smith et al., 2016b; Shields and Mills, 2017; Shields et al., 2020). For the BACE, some recent hypotheses link the down-going limb with input of isotopically light carbon via combined mantle outgassing and organic carbon combustion during rift volcanism, possibly associated the Wichita Igneous Province 'WIP' or related magmatism along the margins of Laurentia (Fig. 4e, Hodgin et al., 2021; Smith et al., 2023). Hydrothermal venting of greenhouse gases from magmatic sills and flows appears to have played an important role in several better constrained Phanerozoic negative $\delta^{13}C$ excursions, such as the Permian-Triassic boundary (Black et al., 2012), Triassic-Jurassic boundary (Ruhl et al., 2011), and Palaeocene-Eocene Thermal Maximum (Berndt et al., 2023). However, while available high-precision radioisotopic ages constrain an extrusive pulse for the WIP to ca. 539 Ma, in advance of negative excursions in both BACE models (Fig. 4), a major phase of intrusive (with some extrusive) WIP volcanism is dated to between ca. 532 Ma and 530 Ma, and instead coincides with overall rising, but unstable, $\delta^{13}C_{carb}$ during recovery from the BACE (Fig. 4e, Wall et al., 2021). Nonetheless, Smith et al. (2023) note that there are significant volumes of poorly constrained rift-related volcanic and magmatic rocks along the margins of Laurentia that broadly coincide with the Ediacaran-Cambrian transition, and this does not account for areas more distal to the continental margin with limited preservation potential.

Alternative models link multi-million-year trends in $\delta^{13}C_{carb}$ data with cycles of global sea level and their underlying drivers (e.g., Brasier and Lindsay, 2001; Bachan et al., 2017; Busch et al., 2022; Bowyer et al., 2024). Second-order eustatic cycles (durations of ca. 5–50 Ma) are dominantly controlled by global plate reorganization and attendant changes in the volume of mid-ocean ridges, as well as isostatic rebound (e.g., Sloss, 1963; Marcilly et al., 2022 and references therein). These underlying tectonic processes influence continental uplift and

erosion, affecting (1) rates of carbonate weathering and deposition, and (2) the balance between oxidation and burial of organic carbon and sulfide on a global scale. Together these factors regulate the steady state carbon cycle by modulating the proportion of carbon buried as organic matter on long timescales (Shields and Mills, 2017). Shorter-term pulses of sulfate delivery via evaporite weathering may also have been important drivers for non-steady state carbon cycle dynamics and oxygenation events in the late Ediacaran (e.g., Shields et al., 2020).

Weathering and erosion not only regulate rates of sulfide and organic carbon oxidation on the continents but also deliver nutrients to marginal marine settings. These nutrients stimulate productivity, which drives marine anoxia and bacterial sulfate reduction (e.g., Shields et al., 2020 and references therein). Neoproterozoic and early Paleozoic marine sediments were deposited under redox stratified water column conditions with oxygenated surface waters overlying anoxic depths (reviewed in Bowyer et al., 2017). Recent modelling also suggests that flooded shelf area was likely a dominant control on pyrite burial throughout the Phanerozoic (Mertens et al., 2025). The numerous high amplitude $\delta^{13}C_{carb}$ excursions across the late Ediacaran and lower Cambrian interval may then be linked, in part, to productivity feedbacks on organic carbon and pyrite burial that were promoted during transgressive flooding of depositional settings by anoxic waters (Brasier and Lindsay, 2001; Bachan et al., 2017 and references therein).

Eustatic sea level not only regulates the global marine shelf area available for efficient burial of organic carbon and pyrite, but also the areal extent of shallow and semi-restricted settings. These shallow settings may exhibit local carbon isotope reservoir effects that have the potential to drive regional variability in the magnitude of $\delta^{13}C_{carb}$ oscillations in some intervals of the preserved Ediacaran rock record (Busch et al., 2022). All of these processes are to some degree influenced by global plate tectonic organization, eustasy and climate, and some combination could have contributed to carbon cycle instability across the Ediacaran-Cambrian transition,

especially given the temporal position of the BACE near the onset of continental flooding associated with the Sauk transgression (Fig. 4e, Brasier and Lindsay, 2001).

Possible drivers for late Ediacaran extinction

The widespread disappearance of Ediacaran soft-bodied biota and numerous skeletal taxa in the late Ediacaran is often proposed to reflect either (or a combination of) rapid and catastrophic mass extinction or gradual biotic replacement (reviewed most recently by Darroch et al., 2023 and Mussini and Dunn, 2024). Below, we discuss how/whether the global compilation may help to address these drivers.

Changes in ocean chemistry and climate, including global warming, oceanic anoxia, and hydrogen sulfide poisoning, have been invoked as plausible mass extinction mechanisms, but high-resolution geochemical proxy datasets to constrain global changes across the BACE and the interval of Ediacaran-Cambrian biotic turnover remain sparse. Recent multi-proxy data from the Turkut Formation of northern Siberia suggest that low oxygen conditions were maintained on both the local and global scales across an interval that may correspond with the lower ENIP (Cherry et al., 2022). This same composite section also hosts the last occurrence of Ediacaran-type soft-bodied fauna and LO of *Cambrotubulus* on the Siberian craton (Nagovitsin et al., 2015). Significant scatter in $\delta^{238}U_{carb}$ data is evident in global Ediacaran-Cambrian temporal correlations (e.g., Bowyer et al., 2024), but the available data trends suggest overall low global marine oxygen levels across the late Ediacaran and early Cambrian. As $\delta^{238}U_{carb}$ is generally interpreted as a proxy for the global extent of seafloor anoxia, these values are relatively insensitive to localized changes in redox conditions on shallow marine shelves (e.g., Lau et al., 2019). Despite the clear need for additional redox proxy data, the disappearance of Ediacaran soft-bodied biota appears to have broadly coincided with a trend towards increasing $\delta^{238}U_{carb}$ (antithetic to the late Ediacaran trend in $\delta^{13}C_{carb}$ in advance of the BACE

547 nadir, Bowyer et al., 2024), which is often interpreted to reflect global oxygenation, rather than
548 deoxygenation.

549 Biotic replacement scenarios for the Ediacaran-Cambrian transition typically draw on the
550 continuum of sediment interaction styles in the late Ediacaran and the attendant increase in
551 trace fossil complexity (e.g., Mángano and Buatois, 2020; Darroch et al., 2021, 2023; Turk et
552 al., 2022; Gougeon et al., 2025a). Ichnotaxa that record shallow bed-penetrative bioturbation
553 co-existed with microbial matgrounds and soft-bodied Ediacaran fauna in numerous terminal
554 Ediacaran environments, alongside biomineralizing cloudinomorphs in co-eval carbonate
555 settings (e.g., Jensen et al., 2000; Buatois et al., 2018; Chen et al., 2018, 2019; Mángano and
556 Buatois, 2020; Nelson et al., 2022; Turk et al., 2022, 2024; Darroch et al., 2021, 2023; Gong
557 et al., 2025). On the Kalahari craton alone, these features co-existed for ≥2 Myrs prior to BACE
558 onset (Fig. 3, Nelson et al., 2022, in press; Gong et al., 2025).

559 ***Evidence for and against late Ediacaran mass extinction***

560 Available geochronological, palaeontological and geochemical proxy datasets are currently
561 too limited to support the argument for a catastrophic mass extinction linked to dramatic
562 changes in oceanic chemistry or climate at the end-Ediacaran. The majority of geochemical
563 datasets indicate that both late Ediacaran and lower Cambrian biota existed for millions of years
564 in marine settings that were characterised by redox stratification and shallow redoxclines (e.g.,
565 Tostevin et al., 2016; Cherry et al., 2022). Not only is there limited geochemical evidence at
566 present to suggest that the disappearance of Ediacaran soft-bodied organisms coincided with
567 an increase in the intensity of anoxia on regional or global scales relative to the preceding
568 interval, but the trace fossil record also appears to document a coincident increase in the
569 diversity of motile forms that would have had higher oxygen demands. While many of these
570 new organisms were likely better adapted to migrate in response to fluctuations in oxygen or
571 hydrogen sulfide levels and temperature conditions, an equally valid argument (made for the

earlier White Sea extinction by Evans et al., 2022) could also be made that soft-bodied taxa might be expected to have had higher survivorship potential due to the lower oxygen demands afforded by their high surface area to volume ratios.

Biotic replacement, on the other hand, is considered to have taken hold over a protracted interval (see Darroch et al., 2023), and the temporal overlap between the burgeoning trace fossil record and apparent decline of soft-bodied taxa in the terminal Ediacaran is intriguing. While a reduction in preservation potential might be expected for any soft-bodied survivors that co-existed with Fortunian trace makers, inferring ecological stress based on low diversity of late Ediacaran soft-bodied assemblages is likely to be skewed by undersampling along with issues of preservation as well as uncertainties in global stratigraphic correlation (e.g., Darroch et al., 2023; Bowyer et al., 2024).

Perhaps most importantly, prior to interpretation of an extinction mechanism, is that the extinction peak recorded in advance of the BACE is likely exaggerated because it corresponds to a reduction in mean generic richness during an interval of very low standing diversity that had been maintained for a protracted interval (Bowyer et al., 2024). This reiterates the frequently asked question of whether the Ediacaran-Cambrian boundary interval hosts a 'mass extinction' at all (see also Darroch et al., 2023 and references therein). It also highlights an often-overlooked issue that requires focused future study: namely, that the rate of turnover remains poorly constrained because it is influenced by inherent uncertainties in global chronostratigraphic correlation (e.g., difficulties in assigning uncertainty estimates for different stratigraphic alignments). This final point underscores the need for continued refinement of the Ediacaran-Cambrian interval, particularly through radioisotopic calibration, investigation of alternative global chronostratigraphic frameworks that leverage all available data, and systematic collection of fossil abundance data.

Outlook

No single section in the geological record contains a complete, globally representative archive. To achieve a holistic view of any interval of Earth history therefore necessitates the collation of, and extrapolation between, multidisciplinary datasets from globally distributed successions and, possibly, a transition away from the focus being solely on specific 'GSSP' sections. This approach exemplifies the inherently international and collaborative endeavor of Earth science research. As data from detailed regional studies are collated into iterative updates to the global age framework, the sequence of events across the Ediacaran-Cambrian transition will continue to come into sharper focus, in turn further elucidating the early history of animal diversification.

Acknowledgements

Contributions F.B. – conceptualization, writing original draft, writing, review and editing, original figure construction; L.N. – conceptualization, writing, review and editing, including figure editing.

Funding FB acknowledges support from UKRI Project EP/Y008790/1. LLN acknowledges support from the Massachusetts Institute of Technology.

References

Ahm, A.-S.C., Husson, J., 2022. Local and Global Controls on Carbon Isotope Chemostratigraphy. *Cambridge University Press.*

Amthor, J.E., Grotzinger, J.P., Schröder, S., Bowring, S.A., Ramezani, J., Martin, M.W., Matter, A., 2003. Extinction of *Cloudina* and *Namacalathus* at the Precambrian-Cambrian boundary in Oman. *Geology* 31, 431–434.

Azizi,A., El Bakhouch, A., El Albani, A., Kirsimäe, K., El Halim, M., El Hariri, K., Erragragui, M., Hafid, A., Vinn, O., 2023. First record of trace fossils in the Ediacaran-

Cambrian transition on the northern Gondwana platform (Anti-Atlas, Morocco). *Precambrian Research* 399, 107227.
Babcock, L.E., Peng, S., Zhu, M., Xiao, S., Ahlberg, P., 2014. Proposed reassessment of the Cambrian GSSP. *Journal of African Earth Sciences* 98, 3–10.
Bachan, A., Lau, K.V., Saltzman, M.R., Thomas, E., Kump, L.R., Payne, J.L., 2017. A model for the decrease in amplitude of carbon isotope excursions across the Phanerozoic. *American Journal of Science* 317, 641–676.
Barr, S.M., White, C.E., Palacios, T., Jensen, S., Van Rooyen, D., Crowley, J.L., 2023. The Terreneuvian MacCodrum Brook section, Mira terrane, Cape Breton Island, Nova Scotia, Canada: age constraints from ash layers, organic-walled microfossils, and trace fossils. *Canadian Journal of Earth Sciences* 60(3), 307–332.
Bengtson, S. 2002. Origin and early evolution of predation. *Paleontological Society Papers* 8, 289–318.
Berndt, C., Planke, S., Alvarez Zarikian, C.A., Frieling, J., Jones, M.T., Millett, J.M., Brinkhuis, H., Bünz, S., Svensen, H.H., Longman, J., Scherer, R.P., 2023. Shallow-water hydrothermal venting linked to the Palaeocene-Eocene Thermal Maximum. *Nature Geoscience* 16(9), 803–809.
Black, B.A., Elkins-Tanton, L.T., Rowe, M.C., Peate, I.U., 2012. Magnitude and consequences of volatile release from the Siberian Traps. *Earth and Planetary Science Letters* 317, 363–373.
Boggiani, P.C., Gaucher, C., Sial, A.N., Babinski, M., Simon, C.M., Riccomini, C., Ferreira, V.P., Fairchild, T.R., 2010. Chemostratigraphy of the Tamengo Formation (Corumbá Group, Brazil): A contribution to the calibration of the Ediacaran carbon-isotope curve. *Precambrian Research* 182, 382–401.
Bold, U., Smith, E.F., Rooney, A.D., Bowring, S.A., Buchwaldt, R., Dudás, F.Ö., Ramezani, J., Crowley, J.L., Schrag, D.P., Macdonald, F.A., 2016. Neoproterozoic stratigraphy of the Zavkhan Terrane of Mongolia: The backbone for Cryogenian and early Ediacaran chemostratigraphic records. *American Journal of Science* 316, 1–63.
Bowring, S.A., Grotzinger, J.P., Condon, D.J., Ramezani, J., Newall, M.J., Allen, P.A., 2007. Geochronologic constraints on the chronostratigraphic framework of the Neoproterozoic Huqf Supergroup, Sultanate of Oman. *American Journal of Science* 307, 1097–1145.
Bowyer, F.T., Wood, R.A., Poulton, S.W., 2017. Controls on the evolution of Ediacaran metazoan ecosystems: a redox perspective. *Geobiology* 15(4), 516–551.
Bowyer, F.T., Zhuravlev, A.Yu., Wood, R., Shields, G.A., Curtis, A., Poulton, S.W., Condon, D.J., Yang, C., Zhu, M., 2022. Calibrating the temporal and spatial dynamics of the Ediacaran-Cambrian radiation of animals. *Earth-Science Reviews* 225, 103913.
Bowyer, F.T., Zhuravlev, A.Yu., Wood, R., Zhao, F., Sukhov, S.S., Alexander, R.D., Poulton, S.W., Zhu, M., 2023a. Implications of an integrated late Ediacaran to early Cambrian stratigraphy of the Siberian Platform, Russia. *Geological Society of America Bulletin* 135(9–10), 2428–2450.
Bowyer, F.T., Uahengo, C.-I., Kaputuaza, K., Ndeunyema, J., Yilales, M., Alexander, R.D., Curtis, A., Wood, R.A., 2023b. Constraining the onset and environmental setting of metazoan biomineralization: The Ediacaran Nama Group of the Tsaus Mountains, Namibia. *Earth and Planetary Science Letters* 620, 118336.
Bowyer, F.T., Wood, R., Yilales, M., 2024. Sea level controls on Ediacaran-Cambrian animal radiations. *Science Advances* 10(31), p.eado6462.
Bowyer, F.T., Messori, F., Wood, R., Linnemann, U., Rojo-Perez, E., Zieger-Hofmann, M., Zieger, J., Ndeunyema, J., Shipanga, M., Mataboge, B., Condon, D., Rose, C.V., Uahengo, C.-I., Gaynor, S.P., Müller, I.A., Geyer, G., Vennemann, T., Davies,

673 J.H.F.L., Ovtcharova, M., 2025. Foundational uncertainties in terminal Ediacaran
674 chronostratigraphy revealed by high-precision zircon U-Pb geochronology of the
675 Nama Group, Namibia. *Earth-Science Reviews* 268, 105169.
676 Brasier, M., Cowie, J., Taylor, M., 1994. Decision on the Precambrian-Cambrian boundary
677 stratotype. *Episodes* 17, 3–8.
678 Brasier, M.D., Shields, G., Kuleshov, V.N., Zhegallo, E.A., 1996. Integrated chemo- and
679 biostratigraphic calibration of early animal evolution: Neoproterozoic-early Cambrian
680 of southwest Mongolia. *Geological Magazine* 133(4), 445–485.
681 Brasier, M., Lindsay, J.F., 2001. Did supercontinental amalgamation trigger the "Cambrian
682 explosion"? *in* Zhuravlev, A.Yu., Riding, R. (eds.) The Ecology of the Cambrian
683 Radiation: New York, Columbia University Press, p.69–89.
684 Brocks, J.J., Nettersheim, B.J., Adam, P., Schaeffer, P., Jarrett, A.J.M., Güneli, N.,
685 Liyanage, T., van Maldegem, L.M., Hallmann, C., Hope, J.M., 2023. Lost world of
686 complex life and the late rise of the eukaryotic crown. *Nature* 618(7966), 767–773.
687 Buatois, L.A., Mángano, M.G., 2016. Ediacaran ecosystems and the dawn of animals. *In*
688 M.G. Mángano, L.A. Buatois (eds) *The Trace-Fossil Record of Major Evolutionary*
689 *Events, volume 1: Precambrian and Paleozoic*, 27–72. *Topics in Geobiology* 39.
690 Dordrecht, The Netherlands. Springer.
691 Buatois, L.A., Almond, J., Mángano, M.G., Jensen, S., Germs, G.J.B., 2018. Sediment
692 disturbance by Ediacaran bulldozers and the roots of the Cambrian explosion.
693 *Scientific Reports* 8, 4514.
694 Busch, J.F., Hodgin, E.B., Ahm, A.-S., Husson, J.M., Macdonald, F.A., Bergmann, K.D.,
695 Higgins, J.A., Strauss, J.V., 2022. Global and local drivers of the Ediacaran Shuram
696 carbon isotope excursion. *Earth and Planetary Science Letters* 579, 117368.
697 Bush, A.M., Payne, J.L., 2021. Biotic and abiotic controls on the Phanerozoic history of
698 marine animal biodiversity. *Annual Review of Ecology, Evolution, and Systematics*
699 52, 269–289.
700 Cai, Y., Xiao, S., Li, G., Hua, H., 2019. Diverse biomineralizing animals in the terminal
701 Ediacaran Period herald the Cambrian explosion. *Geology* 47(4), 380–384.
702 Carlisle, E., Yin, Z., Pisani, D., Donoghue, P.C.J., 2024. Ediacaran origin and Ediacaran-
703 Cambrian diversification of Metazoa. *Science Advances* 10, eadp7161.
704 Cherry, L.B., Gilleaudeau, G.J., Grazhdankin, D.V., Romaniello, S.J., Martin, A.J.,
705 Kaufman, A.J., 2022. A diverse Ediacara assemblage survived under low-oxygen
706 conditions. *Nature Communications* 13, 7306.
707 Chen, Z., Chen, X., Zhou, C., Yuan, X., Xiao, S., 2018. Late Ediacaran trackways produced
708 by bilaterian animals with paired appendages. *Science Advances* 4, eaao6691.
709 Chen, Z., Zhou, C., Yuan, X., Xiao, S., 2019. Death march of a segmented and trilobate
710 bilaterian elucidates early animal evolution. *Nature* 573(7774), 412–415.
711 Condon, D.J., Schoene, B., McLean, N.M., Bowring, S.A., Parrish, R.R., 2015. Metrology
712 and traceability of U-Pb isotope dilution geochronology (EARTHTIME Tracer
713 Calibration Part I). *Geochimica et Cosmochimica Acta* 164, 464–480.
714 Condon, D.J., Schoene, B., Schmitz, M., Schaltegger, U., Ickert, R.B., Amelin, Y., Augland,
715 L.E., Chamberlain, K.R., Coleman, D.S., Connelly, J.N., Corfu, F., Crowley, J.L.,
716 Davies, J.H.F.L., Denyszyn, S.W., Eddy, M.P., Gaynor, S.P., Heaman, L.M.,
717 Huyskens, M.H., Kamo, S., Kasbohm, J., Keller, C.B., MacLennan, S.A., McLean,
718 N.M., Noble, S., Ovtcharova, M., Paul, A., Ramezani, J., Rioux, M., Sahy, D.,
719 Scoates, J.S., Szymanowski, D., Tapster, S., Tichomirowa, M., Wall C.J., Wotzlaw,
720 J.-F., Yang, C., Yin, Q.-Z., 2024. Recommendations for the reporting and
721 interpretation of isotope dilution U-Pb geochronological information. *Geological*
722 *Society of America Bulletin* 136 (9/10), 4233–4251.

Corsetti, F.A., Hagadorn, J.W., 2003. The Precambrian-Cambrian transition in the southern Great Basin, USA. *The Sedimentary Record* 1, 4–8.

Cramer, B.D., Jarvis, I., 2020. Carbon isotope stratigraphy. *Geologic Time Scale 2020*, 309–343. Elsevier.

Darroch, S.A.F., Cribb, A.T., Buatois, L.A., Germs, G.J.B., Kenchington, C.G., Smith, E.F., Mocke, H., O'Neil, G.R., Schiffbauer, J.D., Maloney, K.M., Racicot, R.A., Turk, K.A., Gibson, B.M., Almond, J., Koester, B., Boag, T.H., Tweedt, S.M., Laflamme, M., 2021. The trace fossil record of the Nama Group, Namibia: Exploring the terminal Ediacaran roots of the Cambrian explosion. *Earth-Science Reviews* 212, 103435.

Darroch, S.A., Smith, E.F., Nelson, L.L., Craffey, M., Schiffbauer, J.D., Laflamme, M., 2023. Causes and consequences of end-Ediacaran extinction: an update. *Cambridge Prisms: Extinction* 1, e15.

dos Reis, M., Thawornwattana, Y., Angelis, K., Telford, M.J., Donoghue, P.C.J., Yang, Z., 2015. Uncertainty in the Timing of Origin of Animals and the Limits of Precision in Molecular Timescales. *Current Biology* 25, 1–12.

Dunn, F.S., Liu, A.G., Grazhdankin, D.V., Vixseboxse, P., Flanerry-Sutherland, J., Green, E., Harris, S., Wilby, P.R., Donoghue, P.C.J., 2021. The developmental biology of *Charnia* and the eumetaoan affinity of the Ediacaran rangeomorphs. *Science Advances* 7, eabe0291.

Erwin, D.H., 2021. Developmental capacity and the early evolution of animals. *Journal of the Geological Society* 178(5), pp.jgs2020–245.

Etemad-Saeed, N., Knoll, A.H., Najafi, M., Bergmann, K.D., Haseley, N., Karimi, S., 2021. Carbon isotope chemostratigraphy of a Gondwanan Ediacaran-Cambrian transition, Soltanieh Mountains, northern Iran. *Gondwana Research* 99, 163–177.

Evans, S.D., Tu, C., Rizzo, A., Surprenant, R.L., Boan, P.C., McCandless, H., Marshall, N., Xiao, S., Droser, M.L., 2022. Environmental drivers of the first major animal extinction across the Ediacaran White Sea-Nama transition. *Proceedings of the National Academy of Sciences of the U.S.A.* 119(46), e2207475119.

Fike, D.A., Grotzinger, J.P., 2008. A paired sulfate-pyrite $\delta^{34}S$ approach to understanding the evolution of the Ediacaran-Cambrian sulfur cycle. *Geochimica et Cosmochimica Acta* 72, 2636–2648.

Gehling, J.G., Jensen, S., Droser, M.L., Myrow, P.M., Narbonne, G.M., 2001. Burrowing below the basal Cambrian GSSP, Fortune Head, Newfoundland. *Geological Magazine* 138(2), 213–218.

Germs, G.J.B., 1972. New shelly fossils from Nama Group, South West Africa. *American Journal of Science* 272, 752–761.

Geyer, G., Landing, E., 2017. The Precambrian-Phanerozoic and Ediacaran-Cambrian boundaries: a historical approach to a dilemma. *In* Brasier, A.T., McIlroy, D., McLoughlin, N. (eds) *Earth System Evolution and Early Life: A Celebration of the Work of Martin Brasier*. Geological Society, London, Special Publications 448, 311–349.

Gold, D.A., Runnegar, B., Gehling, J.G., Jacobs, D.K., 2015. Ancestral state reconstruction of ontogeny supports bilaterian affinity for *Dickinsonia*. *Evolution and Development* 17, 315–324.

Gong, Z., Baillie, I., Nelson, L.L., Gerasimov, S.H., Rose, C., Smith, E.F., 2025. Magnetic susceptibility cyclostratigraphy of the lower Schwarzrand Subgroup in southern Namibia refines temporal calibration of late Ediacaran bilaterian radiation. *Global and Planetary Change* 245, 104668.

Gougeon, R., Buatois, L.A., Mángano, M.G., Narbonne, G.M., Laing, B.A., Paz, M., Minter, N.J., 2025a. Environmental and evolutionary controls in animal-sediment interactions at the onset of the Cambrian explosion. *Current Biology* 35(2), 249–264.

Gougeon, R., Mángano, M.G., Buatois, L.A., Narbonne, G.M., Laing, B.A., Paz, M. 2025b. Ichnology of the Ediacaran-Cambrian Chapel Island Formation of Newfoundland, Canada: unraveling bioturbation at the onset of the Cambrian Explosion. *Fossils and Strata* 72, 1–215. Scandinavian University Press. doi: https://doi.org/10.18261/9788294167128-2025

Grotzinger, J., Al-Rawahi, Z., 2014. Depositional facies and platform architecture of microbialite-dominated carbonate reservoirs, Ediacaran-Cambrian Ara Group, Sultanate of Oman. *AAPG Bulletin* 98(8), 1453–1494.

Hamilton, M.A., Álvaro, J.J., Barr, S.M., Jensen, S., Johnson, S.C., Palacios, T., van Rooyen, D., White, C.E., 2023. U-Pb zircon ages from tuffaceous beds in the Terreneuvian to Cambrian Series 2 sections of Avalonian southern New Brunswick, Canada: new constraints on chronostratigraphic correlations and the Cambrian time scale. In Nance, R.D., Strachan, R.A., Quesada, C., Lin, S. (eds.) *Supercontinents, Orogenesis and Magmatism. Geological Society, London, Special Publications* 542.

Hantsoo, K.G., Kaufman, A.J., Cui, H., Plummer, R.E., Narbonne, G.M., 2018. Effects of bioturbation on carbon and sulfur cycling across the Ediacaran-Cambrian transition at the GSSP in Newfoundland, Canada. *Canadian Journal of Earth Sciences* 55(11), 1240–1252.

Hodgin, E.B., Nelson, L.L., Wall, C.J., Barrón-Díaz, A.J., Webb, L.C., Schmitz, M.D., Fike, D.A., Hagadorn, J.W., Smith, E.F., 2021. A link between rift-related volcanism and end-Ediacaran extinction? Integrated chemostratigraphy, biostratigraphy, and U-Pb geochronology from Sonora, Mexico. *Geology* 49, 115–119.

Isachsen, C.E., Bowring, S.A., Landing, E., Samson, S.D., 1994. New constraint on the division of Cambrian time. *Geology* 22, 496–498.

Javaux, E.J., 2019. Challenges in evidencing the earliest traces of life. *Nature* 572(7770), 451–460.

Jensen, S., Saylor, B.Z., Gehling, J.G., Germs, G.J.B., 2000. Complex trace fossils from the terminal Proterozoic of Namibia. *Geology* 28, 143–146.

Jensen, S. Droser, M.L., Heim, N.A., 2002. Trace fossils and ichnofabrics of the lower Cambrian Wood Canyon Formation, southwest Death Valley area. *In* Corsetti, F.A. (Ed.) *Proterozoic-Cambrian of the Great Basin and Beyond*. Field trip guidebook and volume prepared for the Annual Pacific Section SEPM Fall Field Trip, Nov. 15-17, 2002. The Pacific Section SEPM (Society for Sedimentary Geology), Fullerton, California, pp. 123–135.

Karlstrom, K.E., Mohr, M.T., Schmitz, M.D., Sundberg, F.A., Rowland, S.M., Blakey, R., Foster, J.R., Crossey, L.J., Dehler, C.M., Hagadorn, J.W., 2020. Redefining the Tonto Group of Grand Canyon and recalibrating the Cambrian time scale. *Geology* 48(5), 425–430.

Keller, C.B., Schoene, B., Samperton, K.M., 2018. A stochastic sampling approach to zircon eruption age interpretation. *Geochemical Perspective Letters* 8, 31–35.

Keller, M., Lehnert, O., Cooper, J.D., 2012. Sauk megasequence supersequences, southern Great Basin: Second-order accommodation events on the southwestern Cordilleran margin platform, in J. R. Derby, R. D. Fritz, S. A. Longacre, W. A. Morgan, and C. A. Sternbach, eds., The great American carbonate bank: The geology and economic resources of the Cambrian– Ordovician Sauk megasequence of Laurentia: *AAPG Memoir* 98, 873–89

Kouchinsky, A., Bengtson, S., Landing, E., Steiner, M., Vendrasco, M., Ziegler, K., 2017. Terreneuvian stratigraphy and faunas from the Anabar Uplift, Siberia. *Acta Palaeontologica Polonica* 62(2), 311–440.

Knoll, A.H., Grotzinger, J.P., Kaufman, A.J., Kolosov, P., 1995. Integrated approaches to terminal Proterozoic stratigraphy: an example from the Olenek Uplift, northeastern Siberia. *Precambrian Research* 73, 251–270.

Krause, A.J., Mills, B.J.W., Merdith, A.S., Lenton, T.M., Poulton, S.W., 2022. Extreme variability in atmospheric oxygen levels in the late Precambrian. *Science Advances* 8, eabm8191.

Laing, B.A., Mángano, M.G., Buatois, L.A., Narbonne, G.M., Gougeon, R.C., 2019. A protracted Ediacaran-Cambrian transition: an ichnologic ecospace analysis of the Fortunian in Newfoundland, Canada. *Geological Magazine* 156, 1623–1630.

Landing, E., Geyer, G., Brasier, M.D., Bowring, S.A., 2013. Cambrian evolutionary radiation: Context, correlation, and chronostratigraphy – Overcoming deficiencies of the first appearance datum (FAD) concept. *Earth-Science Reviews* 123, 133–172.

Lazar, B., Erez, J., 1990. Extreme ^{13}C depletions in seawater-derived brines and their implications for the past geochemical carbon cycle. *Geology* 18, 1191–1194.

Lau, K.V., Romaniello, S.J., Zhang, F., 2019. The Uranium Isotope Paleoredox Proxy. *In*: Lyons, T., Turchyn, A., Reinhard, C. (Eds.) *Geochemical Tracers in Earth System Science*. Cambridge Elements, pp. 1–28.

Li, D., Ling, H.-F., Shields-Zhou, G.A., Chen, X., Cremonese, L., Och, L., Thirlwall, M., Manning, C.J., 2013. Carbon and strontium isotope evolution of seawater across the Ediacaran-Cambrian transition: Evidence from the Xiaotan section, NE Yunnnan, South China. *Precambrian Research* 225, 128–147.

Li, Z.-X., Liu, Y., Ernst, R., 2023. A dynamic 2000–540 Ma Earth history: From cratonic amalgamation to the age of supercontinent cycle. *Earth-Science Reviews* 238, 104336.

Lindsay, J.F., Brasier, M.D., Dorjnamjaa, D., Goldring, R., Kruse, P.D., Wood, R.A., 1996. Facies and sequence controls on the appearance of the Cambrian biota in southwestern Mongolia: implications for the Precambrian-Cambrian boundary. *Geological Magazine* 133(4), 417–428.

Linnemann, U., Ovtcharova, M., Schaltegger, U., Gärtner, A., Hautmann, M., Geyer, G., Vickers-Rich, P., Rich, T., Plessen, B., Hofmann, M., Zieger, J., Krause, R., Kriesfeld, L., Smith, J., 2019. New high-resolution age data from the Ediacaran-Cambrian boundary indicate rapid, ecologically driven onset of the Cambrian explosion. *Terra Nova* 31(1), 49–58.

Lyons, T.W., Tino, C.J., Fournier, G.P., nderson, R.E., Leavitt, W.D., Konhauser, K.O., Stüeken, E.E., 2024. Co-evolution of early Earth environments and microbial life. *Nature Reviews Microbiology* 22(9), 572–586.

Maloof, A.C., Schrag, D.P., Crowley, J.L., Bowring, S.A., 2005. An expanded record of early Cambrian carbon cycling from the Anti-Atlas Margin, Morocco. *Canadian Journal of Earth Sciences* 42, 2195–2216.

Maloof, A.C., Porter, S.M., Moore, J.L., Dudás, F.Ö., Bowring, S.A., Higgins, J.A., Fike, D.A., Eddy, M.P., 2010. The earliest Cambrian record of animals and ocean geochemical change. *Geological Society of America Bulletin* 122, 1731–1774.

Mángano, M.G., Buatois, L.A., 2020. The rise and early evolution of animals: where do we stand from a trace-fossil perspective? *Interface Focus* 10, 20190103.

Marcilly, C.M., Torsvik, T.H., Conrad, C.P., 2022. Global Phanerozoic sea levels from paleogeographic flooding maps. *Gondwana Research* 110, 128–142.

Marusin, V.V., Kochnev, B.B., Karlova, G.A., Izokh, O.P., Sarsembaev, Zh.A., Ivanova, N.A., 2023. Precambrian-Cambrian transition at the Igarka Uplift (northwestern Siberian Platform). *Russian Geology and Geophysics* 64(6), 682–697.

Marusin, V.V., 2025. Terminal Ediacaran-Terreneuvian revolutions in Siberia. *Earth-Science Reviews* 261, 105009.

Matthews, S.C., Missarzhevsky, V.V., 1975. Small shelly fossils of late Precambrian and early Cambrian age: a review of recent work. *Journal of the Geological Society* 131, 289–303.

Mattinson, J.M., 2005. Zircon U-Pb chemical abrasion ("CA-TIMS") method: Combined annealing and multi-step partial dissolution analysis for improved precision and accuracy of zircon ages. *Chemical Geology* 220, 47–66.

Mertens, C., Paradis, S., Hemingway, J.D., 2025. Sedimentary conditions drive modern pyrite burial flux to exceed oxidation. *Nature Geoscience* https://doi.org/10.1038/s41561-025-01855-5.

Mussini, G., Dunn, F.S., 2024. Decline and fall of the Ediacarans: late-Neoproterozoic extinctions and the rise of the modern biosphere. *Biological Reviews* 99, 110–130.

Myrow, P.M., Hiscott, R.N., 1991. Shallow-water gravity-flow deposits, Chapel Island Formation, southeast Newfoundland, Canada. *Sedimentology* 38, 935-959.

Myrow, P.M., Hiscott, R.N., 1993. Depositional history and sequence stratigraphy of the Precambrian-Cambrian boundary stratotype section, Chapel Island Formation, southeast Newfoundland. *Palaeogeography, Palaeoclimatology, Palaeoecology* 104, 13–35.

Myrow, P.M., Landing, E., 1992. Mixed siliciclastic-carbonate deposition in an early Cambrian oxygen-stratified basin, Chapel Island Formation, southeastern Newfoundland. *Journal of Sedimentary petrology* 62(3), 455–473.

Na, L., Kiessling, W., 2015. Diversity partitioning during the Cambrian radiation. *Proceedings of the National Academy of Sciences of the U.S.A.* 112(15), 4702–4706.

Nagovitsin, K.E., Rogov, V.I., Marusin, V.V., Karlova, G.A., Kolesnikov, A.V., Bykova, N.V., Grazhdankin, D.V., 2015. Revised Neoproterozoic and Terreneuvian stratigraphy of the Lena-Anabar Basin and north-western slope of the Olenek Uplift, Siberian Platform. *Precambrian Research* 270, 226–245.

Narbonne, G.M., Kaufman, A.J., Knoll, A.H., 1994. Integrated chemostratigraphy and biostratigraphy of the Windermere Supergroup, northwestern Canada: Implications for Neoproterozoic correlations and the early evolution of animals. *Geological Society of America Bulletin* 106(10), 1281–1292.

Nelson, L.L., Ramezani, J., Almond, J.E., Darroch, S.A.F., Taylor, W.L., Brenner, D.C., Furey, R.P., Turner, M., Smith, E.F., 2022. Pushing the boundary: A calibrated Ediacaran-Cambrian stratigraphic record from the Nama Group in northwestern Republic of South Africa. *Earth Planet Sci Lett* 580, 117396.

Nelson, L.L., Crowley, J.L., Smith, E.F., Schwartz, D.M., Hodgin, E.B., Schmitz, M.D., 2023. Cambrian explosion condensed: High-precision geochronology of the lower Wood Canyon Formation, Nevada. *Proceedings of the National Academy of Sciences of the United States of America* 120, e2301478120.

Nelson, L.L., Smith, E.F., Darroch, S.A.F., Baillie, I., Ramezani, J., Almond, J.E., Swart, R., Polomski, D.E., Turk, K.A, *in press*, A Basin in Transition: Ecological, Environmental, and Tectonic Shifts Across the Ediacaran–Cambrian Boundary in the Nama Group, Kalahari Craton. *American Journal of Science*. https://doi.org/10.2475/001c.151699

Park, Y., Swanson-Hysell, N.L., MacLennan, S.A., Maloof, A.C., Gebreslassie, M., Tremblay, M.M., Schoene, B., Alene, M., Anttila, E.S.C., Tesema, T., Haileab, B.,

2020. The lead-up to the Sturtian Snowball Earth: Neoproterozoic chemostratigraphy time-calibrated by the Tambien Group of Ethiopia. *Geological Society of America Bulletin* 132(5/6), 1119–1149.

Parry, L.A., Boggiani, P.C., Condon, D.J., Garwood, R.J., Leme, J.D.M., McIlroy, D., Brasier, M.D., Trindade, R., Campanha, G.A.C., Pacheco, M.L.A.F., Diniz, C.Q.C., Liu, A.G., 2017. Ichnological evidence for meiofaunal bilaterians from the terminal Ediacaran and earliest Cambrian of Brazil. *Nature Ecology and Evolution* 1, 1455–1464.

Ramezani, J., Hoke, G.D., Fastovsky, D.E., Bowring, S.A., Therrien, F., Dworkin, S.I., Atchley, S.C., Nordt, L.C., 2011. High-precision U-Pb zircon geochronology of the Late Triassic Chinle Formation, Petrified Forest National Park (Arizona, USA): Temporal constraints on the early evolution of dinosaurs. *Geological Society of America Bulletin* 123(11/12), 2142–2159.

Ramos, M.E.A.F., Giorgioni, M., Walde, D.H.G., do Carmo, D.A., Fazio, G., Vieira, L.C., Denezine, M., Santos, R.V., Adôrno, R.R., Guida, L.L., 2022. New facies model and carbon isotope stratigraphy for an Ediacaran carbonate platform from South America (Tamengo Formation – Corumbá Group, SW Brazil). *Frontiers in Earth Science* 10, 749066.

Rohde, R.A., Muller, R.A., 2005. Cycles in fossil diversity. *Nature* 434, 208–210.

Ruhl, M., Bonis, N.R., Reichart, G.-J., Damsté, J.S.S., Kürschner, W.M., 2011. Atmospheric Carbon Injection Linked to End-Triassic Mass Extinction. *Science* 333(6041), 430–434.

Runnegar, B., Gehling, J.G., Horodyski, R.J., Jensen, S. Knauth, L.P. 1995. Base of the Sauk sequence is a global eustatic event that lies just above the Precambrian-Cambrian boundary. *Geological Society of America, Abstracts with Programs* 270, A-330.

Runnegar, B., Horodyski, R.J., Gehling, J.G., Jensen, S., Bengtson, S., Peterson, K.J., Saltzman, M.R., Vendrasco, MJ., 2025. *Tulaneia amabilia* n. gen. n. sp.: a new erniettomorph from the Wood Canyon Formation, Nevada and the age of the Ediacaran–Cambrian transition in the Great Basin. *Journal of Paleontology* 98, 929–951.

Saylor, B.Z., Kaufman, A.J., Grotzinger, J.P., Urban, F., 1998. A composite reference section for terminal Proterozoic strata of southern Namibia. *Journal of Sedimentary Research* 68(6), 1223–1235.

Selly, T., Schiffbauer, J.D., Jacquet, S.M., Smith, E.F., Nelson, L.L., Andreasen, B.D., Huntley, J.W., Strange, M.A., O'Neil, G.R., Thater, C.A., Bykova, N., Steiner, M., Yang, B., Cai, Y., 2020. A new cloudinid fossil assemblage from the terminal Ediacaran of Nevada, USA. *Journal of Systematic Palaeontology* 18(4), 357–379.

Schaltegger, U., Schmitt, A.K., Horstwood, M.S.A., 2015. U-Th-Pb zircon geochronology by ID-TIMS, SIMS, and laser ablation ICP-MS: Recipes, interpretations, and opportunities. *Chemical Geology* 402, 89–110.

Schiffbauer, J.D., Wong, C., David, C., Selly, T., Nelson, L.L., Pruss, S.B., 2024. Reassessing the diversity, affinity, ad construction of terminal Ediacaran tubiform fossils from the La Ciénega Formation, Sonora, Mexico. *Journal of Paleontology* 98(2), 266–282.

Schrag, D.P., Higgins, J.A., Macdonald, F.A., Johnston, D.T., 2013. Authigenic carbonate and the history of the global carbon cycle. *Science* 339(6119), 540–543.

Schröder, S., Grotzinger, J.P., Amthor, J.E., Matter, A., 2005. Carbonate deposition and hydrocarbon reservoir development at the Precambrian-Cambrian boundary: The Ara Group in South Oman. *Sedimentary Geology* 180, 1–28.

Schröder, S., Grotzinger, J.P., 2007. Evidence for anoxia at the Ediacaran-Cambrian boundary: the record of redox-sensitive trace elements and rare earth elements in Oman. *Journal of the Geological Society, London* 164, 175–187.

Shahkarami, S., Buatois, L.A., Mángano, M.G., Hagadorn, J.W., Almond, J., 2020. The Ediacaran-Cambrian boundary: Evaluating stratigraphic completeness and the Great Unconformity. *Precambrian Research* 345, 105721.

Shields, G.A., Mills, B.J.W., 2017. Tectonic controls on the long-term carbon isotope mass balance. *Proceedings of the National Academy of Sciences of the United States of America* 114(17), 4318–4323.

Shields, G.A., Mills, B.J.W., Zhu, M., Raub, T.D., Daines, S.J., Lenton, T.M., 2020. Unique Neoproterozoic carbon isotope excursions sustained by coupled evaporite dissolution and pyrite burial. *Nature Geoscience* 12, 823–827.

Sloss, L.L., 1963. Sequences in the cratonic interior of North America. *Geological Society of America Bulletin* 74, 93–114.

Smith, E.F., Nelson, L.L., Strange, M.A., Eyster, A.E., Rowland, S.M., Schrag, D.P., Macdonald, F.A., 2016a. The end of the Ediacaran: Two new exceptionally preserved body fossil assemblages from Mount Dunfee, Nevada, USA. *Geology* 44(11), 911–914.

Smith, E.F., Macdonald, F.A., Petach, T.A., Bold, U., Schrag, D.P., 2016b. Integrated stratigraphic, geochemical, and paleontological late Ediacaran to early Cambrian records from southwestern Mongolia. *Geological Society of America Bulletin* 128(3-4), 442–468.

Smith, E.F., Nelson, L.L., Tweedt, S.M., Zeng, H., Workman, J.B., 2017. A cosmopolitan late Ediacaran biotic assemblage: new fossils from Nevada and Namibia support a global biostratigraphic link. *Proceedings of the Royal Society B* 284, 20170934.

Smith, E.F., Nelson, L.L., O'Connell, N., Eyster, A., Lonsdale, M.C., 2023. The Ediacaran-Cambrian transition in the southern Great Basin, United States. *Geological Society of America Bulletin* 135(5-6), 1393–1414.

Steiner, M., Li, G., Qian, Y., Zhu, M., Erdtmann, B.-D., 2007. Neoproterozoic to early Cambrian small shelly fossil assemblages and a revised biostratigraphic correlation of the Yangtze Platform (China). *Palaeogeography, Palaeoclimatology, Palaeoecology* 254, 67–99.

Stockey, R.G., Cole, D.B., Farrell, U.C., Agíc, H., Boag, T.H., Brocks, J.J., Canfield, D.E., Cheng, M., Crockford, P.W., Cui, H., Dahl, T.W., Mouro, L.D., Dewing, K., Dornbos, S.Q., Emmings, J.F., Gaines, R.R., Gibson, T.M., Gill, B.C., Gilleaudeau, G.J., Goldberg, K., Guilbaud, R., Halverson, G., Hammarlund, E.U., Hantsoo, K., Henderson, M.A., Henderson, C.M., Hodgskiss, M.S.W., Jarrett, A.J.M., Johnston, D.T., Kabanov, P., Kimmig, J., Knoll, A.H., Kunzmann, M., LeRoy, M.A., Li, C., Loydell, D.K., Macdonald, F.A., Magnall, J.M., Mills, N.T., Och, L.M., O'Connell, B., Pagès, A., Peters, S.E., Porter, S.M., Poulton, S.W., Ritzer, S.R., Rooney, A.D., Schoepfer, S., Smith, E.F., Strauss, J.V., Uhlein, G.J., White, T., Wood, R.A., Woltz, C.R., Yurchenko, I., Planavsky, N.J., Sperling, E.A., 2024. Sustained increases in atmospheric oxygen and marine productivity in the Neoproterozoic and Palaeozoic eras. *Nature Geoscience* 17(7), 667–674.

Sundell, K.E., Macdonald, F.A., 2022. The tectonic context of hafnium isotopes in zircon. *Earth and Planetary Science Letters* 584, 117426,

Szymanowski, D., Wotzlaw, J.-F., Ovtcharova, M., Schoene, B., Schaltegger, U., Schmitz, M., Ickert, R.B., Chelle-Michou, C., Chamberlain, K.R., Crowley, J.L., Davies, J., Eddy, M.P., Gaynor, S., Käßner, A., Mohr, M.T., Paul, A.N., Ramezani, R., Tapster, S., Tichomirowa, M., von Quadt, A., Wall, C.J., 2025. Interlaboratory reproducibility

of ID-TIMS U-Pb geochronology evaluated with a pre-spiked natural zircon solution. *Geochronology* 7(3), 409–425.

Tang, Q., Zheng, W., Zhang, S., Fan, J., Riedman, L.A., Hou, X., Muscente, A.D., Bykova, N., Sadler, P.M., Wang, X., Zhang, F., Yuan, X., Zhou, C., Wan, B., Pang, K., Ouyang, Q., McKenzie, N.R., Zhao, G., Shen, S., Xiao, S., 2024. Quantifying the global biodiversity of Proterozoic eukaryotes. *Science* 386, 1364.

Tarhan, L.G., Myrow, P.M., Smith, E.F., Nelson, L.L., Sadler, P.M., 2020. Infaunal augurs of the Cambrian explosion: An Ediacaran trace fossil assemblage from Nevada, USA. *Geobiology* 18, 486–496.

Tasistro-Hart, A.R., Macdonald, F.A., 2023. Phanerozoic flooding of North America and the Great Unconformity. *Proceedings of the National Academy of Sciences of the United States of America* 120(37), e2309084120.

Topper, T., Betts, M.J., Dorjnamjaa, D., Li, G., Li, L., Altanshagai, G., Enkhbaatar, B., Skovsted, C.B., 2022. Locating the BACE of the Cambrian: Bayan Gol in southwestern Mongolia and global correlation of the Ediacaran-Cambrian boundary. *Earth-Science Reviews* 229, 104017.

Tostevin, R., Wood, R.A., Shields, G.A., Poulton, S.W., Guilbaud, R., Bowyer, F., Penny, A.M., He, T., Curtis, A., Hoffmann, K.H., Clarkson, M.O., 2016. Low-oxygen waters limited habitable space for early animals. *Nature Communications* 7(1), 12818.

Turk, K.A., Maloney, K.M., Laflamme, M., Darroch, S.A., 2022. Paleontology and ichnology of the late Ediacaran Nasep–Huns transition (Nama Group, southern Namibia). *Journal of Paleontology* 96, 753–769.

Turk, K.A., Wehrmann, A., Laflamme, M., Darroch, S.A.F., 2024. Priapulid neoichnology, ecosystem engineering, and the Ediacaran-Cambrian transition. *Palaeontology* 67(4), e12721.

Wall, C.J., Hanson, R.E., Schmitz, M., Price, J.D., Donovan, R.N., Boro, J.R., Eschberger, A.M., Toews, C.E., 2021. Integrating zircon trace-element geochemistry and high-precision U-Pb zircon geochronology to resolve the timing and petrogenesis of the late Ediacaran-Cambrian Wichita igneous province, Southern Oklahoma Aulacogen, USA. *Geology* 49, 268–272.

Wang, Q., Dai, Q., Vayda, P., Luo, J., Shao, T., Liu, Y., Hua, H., Xiao, S., 2025. Fortunian archaeocyath sponges acquired biomineralization in the beginning of the Cambrian explosion. *Geology*. https://doi .org /10 .1130 /G53249 .1

Wood, R., Ivantsov, A.Yu, Zhuravlev, A.Yu., 2017. First macrobiota biomineralization was environmentally triggered. *Proceedings of the Royal Society B* 284, 20170059.

Yang, B., Steiner, M., Zhu, M., Li, G., Liu, J., Liu, P., 2016. Transitional Ediacaran-Cambrian small skeletal fossil assemblages from South China and Kazakhstan: Implications for chronostratigraphy and metazoan evolution. *Precambrian Research* 285, 202–215.

Yang, B., Steinger, M., Schiffbauer, J.D., Selly, T., Wu, X., Zhang, C., Liu, P., 2020. Ultrastructure of Ediacaran cloudinids suggests diverse taphonomic histories and affinities with non-biomineralized annelids. *Scientific Reports* 10(1), 535.

Yang, B., Warren, L.V., Steiner, M., Smith, E.F., Liu, P., 2021. Taxonomic revision of Ediacaran tubular fossils: *Cloudina*, *Sinotubulites* and *Conotubus*. *Journal of Paleontology* 96(2), 256–273.

Yang, C., Rooney, A.D., Condon, D.J., Li, X.-H., Grazhdankin, D.V., Bowyer, F.T., Hu, C., Macdonald, F.A., Zhu, M., 2021. The tempo of Ediacaran evolution. *Science Advances* eabi9643.

Yang, C., Bowyer, F., Condon, D., 2025. High-precision CA-ID-TIMS zircon U-Pb geochronology: A review of the Neoproterozoic time scale. *National Science Review*, p.nwaf206.

Zhang, K., Shields, G.A., Zhou, Y., Strauss, H., Struck, U., Jensen, S., 2024. The basal Cambrian carbon isotope excursion revealed in the Central Iberian Zone, Spain. *Precambrian Research* 411, 107526.

Zhu, M.Y., Babcock, L.E., Peng, S.C., 2006. Advances in Cambrian stratigraphy and paleontology: integrating correlation techniques, paleobiology, taphonomy and paleoenvironmental reconstruction. *Palaeoworld* 15, 217–222.

Zhu, M., Zhuravlev, A.Y., Wood, R.A., Zhao, F., Sukhov, S.S., 2017. A deep root for the Cambrian explosion: Implications of new bio- and chemostratigraphy from the Siberian Platform. *Geology* 45, 459–462.

Zhuravlev, A.Yu., 1986. Evolution of archaeocyaths and palaeobiogeography of the Early Cambrian. *Geological Magazine* 123, 377–385.

Figures

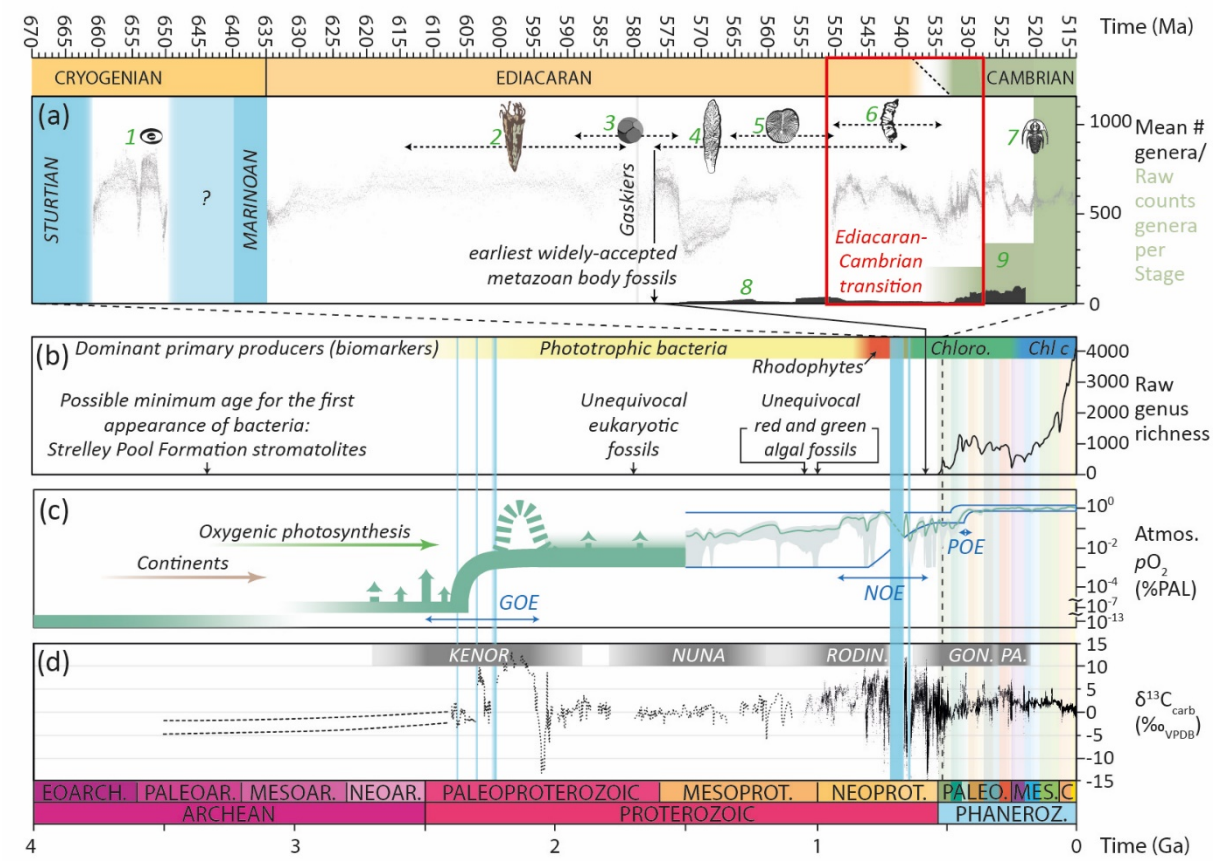
Time (Ma)
CRYOGENIAN
EDIACARAN
CAMBRIAN
(a)
STURTIAN
MARINOAN
Gaskiers
earliest widely-accepted metazoan body fossils
Ediacaran-Cambrian transition
Mean # genera/ Raw counts genera per Stage
(b)
Dominant primary producers (biomarkers)
Phototrophic bacteria
Rhodophytes
Chloro.
Chl c
Possible minimum age for the first appearance of bacteria: Strelley Pool Formation stromatolites
Unequivocal eukaryotic fossils
Unequivocal red and green algal fossils
Raw genus richness
(c)
Oxygenic photosynthesis
Continents
GOE
NOE
POE
Atmos. pO_2 (%PAL)
(d)
KENOR.
NUNA
RODIN.
GON.
PA.
$\delta^{13}C_{carb}$ (‰$_{VPDB}$)
EOARCH.
PALEOAR.
MESOAR.
NEOAR.
PALEOPROTEROZOIC
MESOPROT.
NEOPROT.
PALEO.
MES.
C
ARCHEAN
PROTEROZOIC
PHANEROZ.
Time (Ga)

Fig. 1. Summary figure to show the macroevolutionary significance of the Ediacaran-Cambrian transition. (a) Expanded view of the Cryogenian through lower Cambrian (670-514 Ma) showing key macrofossil occurrences and assemblages: 1. 'Twitya disks' of the mid-Cryogenian (Burzynski et al., 2020); 2. Lantian assemblage of South China; 3. Weng'an assemblage of South China; 4. Avalon assemblage, including the first appearance of macrofossils that are generally agreed to include metazoans (e.g., Dunn et al., 2021); 5. White Sea assemblage, including the earliest bilateraliomorphs; 6. Nama assemblage, including first widespread appearance of animal biomineralization and tubular cloudinomorphs; 7. Lowest occurrence of trilobites in Siberia, approximately coincides with unratified Cambrian Stage 2-3 boundary; 8. Reconstructed mean generic richness (black polygon, with Cambrian mean generic richness estimated using skeletal metazoan data only, terminated at 522 Ma) based on temporally calibrated occurrence dataset (Bowyer et al., 2024); 9. Raw counts of metazoan genera per Stage (green boxes) after Na and Kiessling (2015). Background carbonate carbon isotope composite temporally calibrated using available radioisotopic ages (full data and references in Yang et al., 2021; Bowyer et al., 2023b, 2024, 2025; Nelson et al., 2023, in press; and this study). Vertical blue lines show ages and durations of Proterozoic Snowball Earth glaciations and vertical coloured barcode in right of panels (a)-(c) delineates Series of the Phanerozoic. **(b)** Selected major evolutionary events through geologic time (after Javaux, 2019 and Tang et al., 2024, and references therein), transitions in dominant primary producers (after Brocks et al., 2023), and raw genus richness from Sepkoski's compendium (after Bush and Payne, 2021 with data from Rohde and Muller, 2005). **(c)** Hypothesized trajectory of atmospheric oxygen concentration through geologic time based on multiple geochemical proxy and modelling data (modified after Krause et al., 2022; Lyons et al., 2024 and references therein). Vertical blue bars show hypothesized transitional intervals/episodes of increasing environmental oxygenation: GOE: Great Oxidation Episode; NOE: Neoproterozoic

Oxygenation Event/Episode; POE: Paleozoic Oxygenation Event/Episode. **(d)** Composite carbonate carbon isotope record from multiple previous data compilations (Cramer and Jarvis, 2020; Park et al., 2020; Yang et al., 2021; Bowyer et al., 2023b, 2024, and references therein) with timing of rifting-tenure-breakup of supercontinents after Sundell and Macdonald (2022): Rodin. - Rodinia; Gon. - Gondwana; Pa. - Pangea.

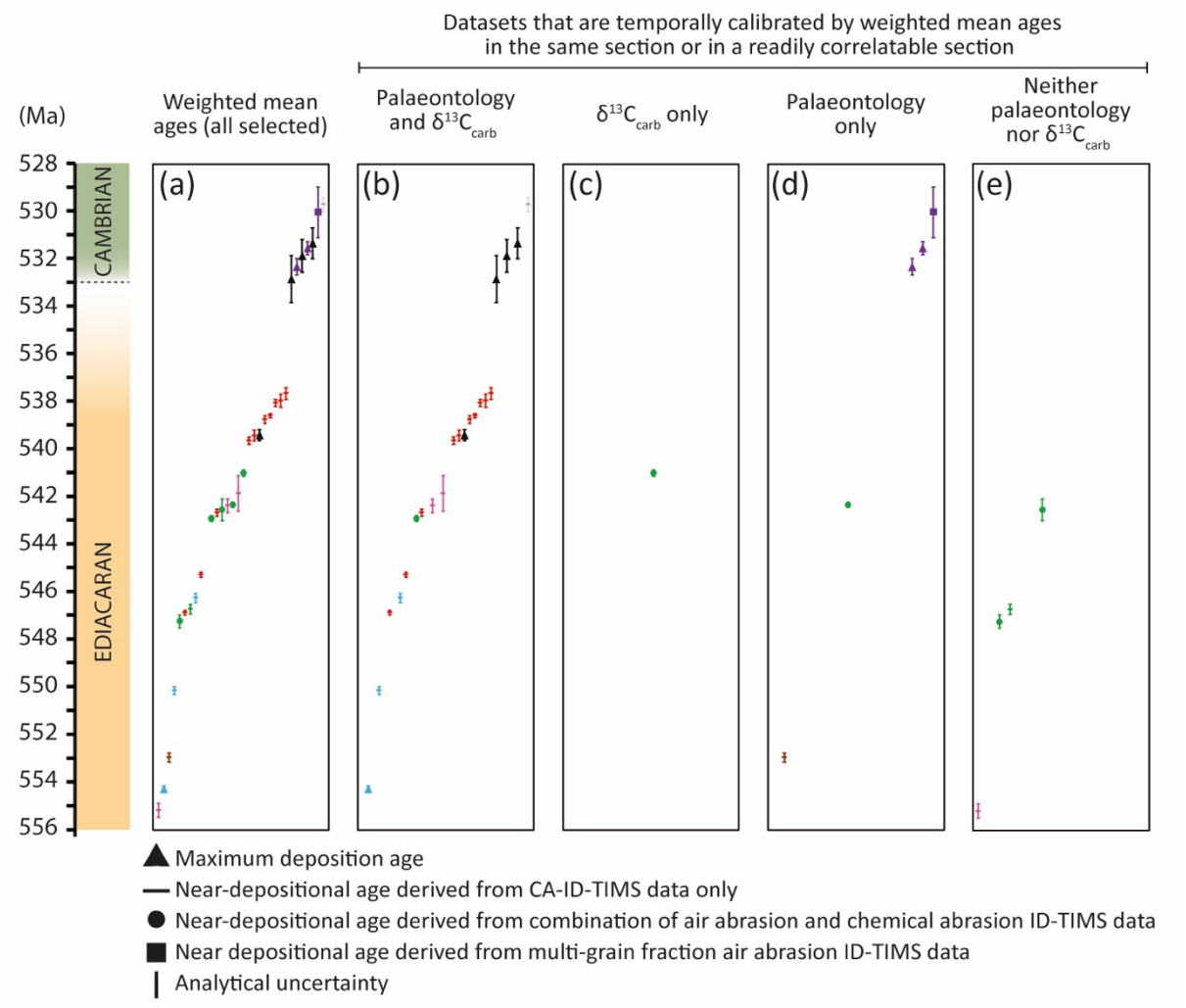

Fig. 2. Available high-precision zircon U-Pb dates for a selection of key stratigraphic sections across the Ediacaran-Cambrian transition and their interpreted chronostratigraphic utility for calibration of chemostratigraphic and fossil occurrence data. All ash bed data are weighted mean ID-TIMS $^{206}Pb/^{238}U$ dates with vertical bars showing 2*s* analytical uncertainties (not accounting for tracer calibration and ^{238}U decay constant uncertainties). However, note that some dates interpreted as near-depositional ages are derived from air abrasion or combined air abrasion and chemical abrasion single grain data, and should be treated with caution. Selected maximum depositional ages (Spring Mountains, Nelson et al., 2023) are calculated from the mode of youngest zircon dates, which does not assume a single magmatic population in case of detrital/reworked grains. Full zircon database and references provided in Table S1. Colours correspond to data provenance, as shown in figure 3, with additional zircon U-Pb ages from South China in blue (see Table S1 for full dataset).

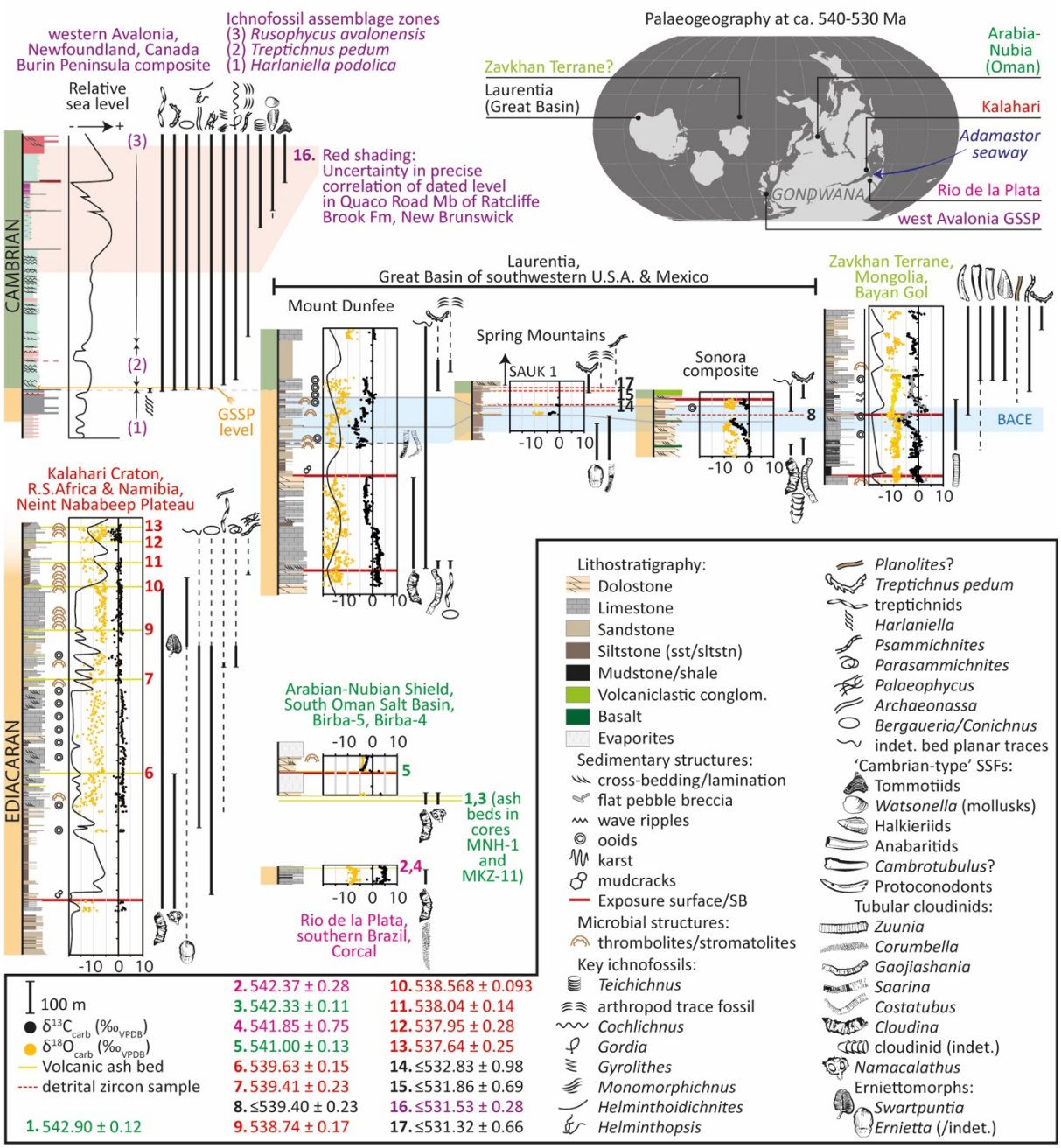
western Avalonia,
Newfoundland, Canada
Burin Peninsula composite
Ichnofossil assemblage zones
(3) Rusophycus avalonensis
(2) Treptichnus pedum
(1) Harlaniella podolica
Relative sea level
CAMBRIAN
EDIACARAN
(3)
(2)
(1)
GSSP level
16. Red shading: Uncertainty in precise correlation of dated level in Quaco Road Mb of Ratcliffe Brook Fm, New Brunswick
Palaeogeography at ca. 540-530 Ma
Zavkhan Terrane?
Laurentia
(Great Basin)
Arabia-
Nubia
(Oman)
Kalahari
Adamastor
seaway
GONDWANA
Rio de la Plata
west Avalonia GSSP
Laurentia,
Great Basin of southwestern U.S.A. & Mexico
Mount Dunfee
Spring Mountains
SAUK 1
Sonora
composite
Zavkhan Terrane,
Mongolia,
Bayan Gol
BACE
Kalahari Craton,
R.S.Africa & Namibia,
Neint Nababeep Plateau
Arabian-Nubian Shield,
South Oman Salt Basin,
Birba-5, Birba-4
1,3 (ash beds in cores MNH-1 and MKZ-11)
Rio de la Plata,
southern Brazil,
Corcal
100 m
δ13Ccarb (‰VPDB)
δ18Ocarb (‰VPDB)
Volcanic ash bed
detrital zircon sample
1. 542.90 ± 0.12
2. 542.37 ± 0.28
3. 542.33 ± 0.11
4. 541.85 ± 0.75
5. 541.00 ± 0.13
6. 539.63 ± 0.15
7. 539.41 ± 0.23
8. ≤539.40 ± 0.23
9. 538.74 ± 0.17
10. 538.568 ± 0.093
11. 538.04 ± 0.14
12. 537.95 ± 0.28
13. 537.64 ± 0.25
14. ≤532.83 ± 0.98
15. ≤531.86 ± 0.69
16. ≤531.53 ± 0.28
17. ≤531.32 ± 0.66
Lithostratigraphy:
Dolostone
Limestone
Sandstone
Siltstone (sst/sltstn)
Mudstone/shale
Volcaniclastic conglom.
Basalt
Evaporites
Sedimentary structures:
cross-bedding/lamination
flat pebble breccia
wave ripples
ooids
karst
mudcracks
Exposure surface/SB
Microbial structures:
thrombolites/stromatolites
Key ichnofossils:
Teichichnus
arthropod trace fossil
Cochlichnus
Gordia
Gyrolithes
Monomorphichnus
Helminthoidichnites
Helminthopsis
Planolites?
Treptichnus pedum
treptichnids
Harlaniella
Psammichnites
Parasammichnites
Palaeophycus
Archaeonassa
Bergaueria/Conichnus
indet. bed planar traces
'Cambrian-type' SSFs:
Tommotiids
Watsonella (mollusks)
Halkieriids
Anabaritids
Cambrotubulus?
Protoconodonts
Tubular cloudinids:
Zuunia
Corumbella
Gaojiashania
Saarina
Costatubus
Cloudina
cloudinid (indet.)
Namacalathus
Erniettomorphs:
Swartpuntia
Ernietta (/indet.)

1126

Fig. 3. Important terminal Ediacaran to lower Cambrian sections that are calibrated (or readily correlatable to sections that are calibrated) by zircon U-Pb ID-TIMS ages (coloured numbers without parentheses). Also shown are the composite section of the Burin Peninsula, Newfoundland, which hosts the ratified basal Cambrian GSSP section at Fortune Head, and one section from the Zavkhan Terrane of Mongolia, neither of which are directly calibrated via radioisotope geochronology. All sections are shown to the same scale. Sediments of the dominantly siliciclastic Burin Peninsula composite section are differentiated by colour. References for lithostratigraphic, geochemical and radioisotopic data: western Avalonia composite (Myrow and Hiscott, 1991, 1993; Myrow and Landing, 1992; Hantsoo et al., 2018; Laing et al., 2019; Gougeon et al., 2025a, b; Hamilton et al., 2023); Neint Nababeep Plateau (Nelson et al., 2022, in press); Great Basin, Laurentia (Smith et al., 2016a, 2023; Selly et al., 2020; Tarhan et al., 2020; Hodgin et al., 2021; Nelson et al., 2023); Zavkhan Terrane (Smith et al., 2016b; Topper et al., 2022); Rio de la Plata craton (Boggiani et al., 2003; Parry et al., 2017; Ramos et al., 2022); Oman (Amthor et al., 2003; Schröder et al., 2005; Bowring et al., 2007; Schröder and Grotzinger, 2007; Fike and Grotzinger, 2008; Grotzinger and Al-Rawahi, 2014). Inset palaeogeography after Li et al. (2023). Ediacaran-Cambrian colour coding is based on lowest occurrence of *T. pedum* in each section but note ambiguity in assignment of the boundary level in the Ara Group of the South Oman Salt Basin and at Bayan Gol section of the Zavkhan Terrane, Mongolia, without employing correlation based on auxiliary chemostratigraphic data. Dashed vertical lines show range extensions of fossil occurrences based on readily correlatable sections or uncertain fossil assignments in the same section. Solid vertical curved lines indicate interpreted relative sea level variations.

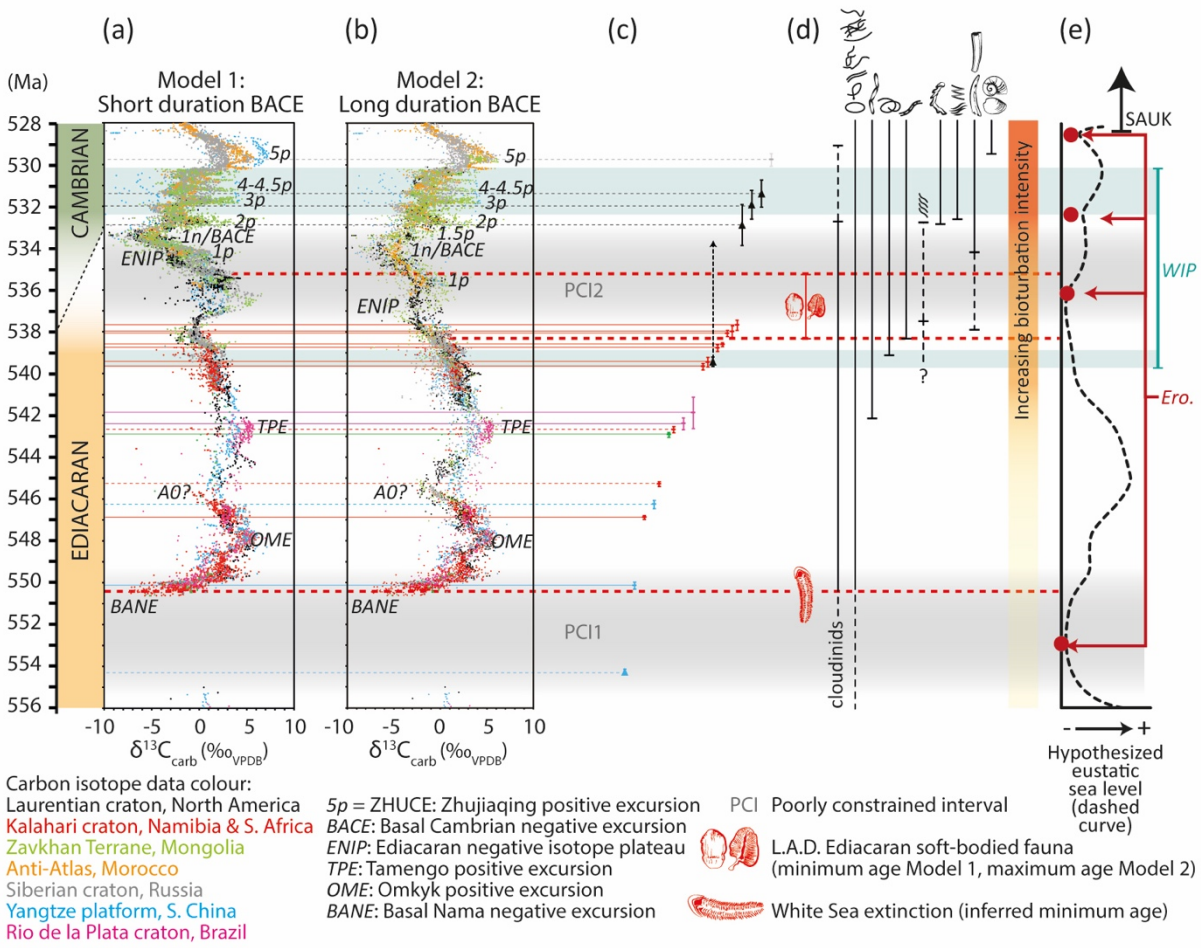
(a)
(b)
(c)
(d)
(e)
(Ma)
Model 1:
Short duration BACE
Model 2:
Long duration BACE
CAMBRIAN
EDIACARAN
5p
4-4.5p
3p
2p
1.5p
1n/BACE
1p
ENIP
TPE
A0?
OME
BANE
PCI2
PCI1
cloudinids
Increasing bioturbation intensity
SAUK
WIP
Ero.
δ13Ccarb (‰VPDB)
Hypothesized eustatic sea level (dashed curve)
Carbon isotope data colour:
Laurentian craton, North America
Kalahari craton, Namibia & S. Africa
Zavkhan Terrane, Mongolia
Anti-Atlas, Morocco
Siberian craton, Russia
Yangtze platform, S. China
Rio de la Plata craton, Brazil
5p = ZHUCE: Zhujiaqing positive excursion
BACE: Basal Cambrian negative excursion
ENIP: Ediacaran negative isotope plateau
TPE: Tamengo positive excursion
OME: Omkyk positive excursion
BANE: Basal Nama negative excursion
PCI Poorly constrained interval
L.A.D. Ediacaran soft-bodied fauna
(minimum age Model 1, maximum age Model 2)
White Sea extinction (inferred minimum age)

1150

Fig. 4. Two possible global chronostratigraphic frameworks that cover the terminal Ediacaran through lowermost Cambrian (Fortunian and lower Stage 2), with associated diversity metrics for Model 1 from Bowyer et al. (2024) and calculated using range-through data. **(a)** A Short-duration interpretation for the BACE (Model 1) follows Nelson et al. (2023) and Bowyer et al. (2024). **(b)** Long-duration BACE (Model 2) is provided here (Table S2). These models are endmember interpretations that comply with existing chronostratigraphic constraints rather than being the only possibilities. **(c)** Radioisotopic ages that temporally calibrate intervals of the global chemostratigraphic correlation. Grey faded horizontal bands highlight poorly constrained intervals (PCI). **(d)** Different extents of biotic assemblage overlap are calibrated within each age framework. Black – BACE Model 1; brown – BACE Model 2. Symbols from Figure 3. Dashed lines show possible range extensions based on additional uncertainties in both chronostratigraphic frameworks [e.g., *Cloudina* extension to lower Stage 2 based on minimum possible age of upper Ust'-Yudoma Formation at Kyra Ytyga section, southeast Siberia (Zhu et al., 2017) as described in Bowyer et al. (2023a)]. See figure 3 for key to black fossil symbols. Ranges for some ichnogenera extend into the Avalon/White Sea interval (>550 Ma) based on occurrence database of Mángano and Buatois (2020). **(e)** Interpreted eustatic sea level curve (dashed line) based on integrated analysis of relative sea level curves from regional composite sections and interpretation of regional tectonic controls. Age constraints for bimodal volcanism associated with emplacement of the Wichita igneous province (WIP, turquoise horizontal bars) after Wall et al. (2021). Ero. - intervals of widespread erosion during maximum eustatic regression.